Phenomenological position and energy resolving Lindblad approach to quantum kinetics

Kiršanskas, Gediminas; Franckié, Martin; Wacker, Andreas

Published in:
Physical Review B

DOI:
10.1103/PhysRevB.97.035432

2018

Document Version:
Publisher's PDF, also known as Version of record

Phenomenological position and energy resolving Lindblad approach to quantum kinetics

Gediminas Kiršanskas, Martin Franckié,* and Andreas Wacker
Mathematical Physics and NanoLund, Lund University, Box 118, 22100 Lund, Sweden

(Received 20 October 2017; published 22 January 2018)

A general theoretical approach to study the quantum kinetics in a system coupled to a bath is proposed. Starting with the microscopic interaction, a Lindblad master equation is established, which goes beyond the common secular approximation. This allows for the treatment of systems, where coherences are generated by the bath couplings while avoiding the negative occupations occurring in the Bloch-Wangsness-Redfield kinetic equations. The versatility and accuracy of the approach is verified by its application to three entirely different physical systems: (i) electric transport through a double-dot system coupled to electronic reservoirs, (ii) exciton kinetics in coupled chromophores in the presence of a heat bath, and (iii) the simulation of quantum cascade lasers, where the coherent electron transport is established by scattering with phonons and impurities.

DOI: 10.1103/PhysRevB.97.035432

I. INTRODUCTION

The dynamical behavior of quantum systems coupled to a bath is a central question for a wide range of physical problems. The classical example is the evolution of a spin in a time-dependent magnetic field in the presence of thermal excitations of the hosting material [1]. Other examples, just to mention a few, are as follows: transport of electrons through quantum dot systems, where the bath is constituted by connecting electron reservoirs at given temperature and electrochemical potential [2–5]; kinetics of excitons in molecular aggregates with their coupling to the vibrations [6,7]; electron transport in extended semiconductor heterostructures, such as superlattices [8–10] or quantum cascade lasers [11,12], where the energy relaxation due to phonon scattering is crucial.

In general, the state of the quantum system can be described by the reduced density operator $\hat{\rho}$ of the system (which is the full density operator after tracing out the degrees of freedom from the baths). Thus, the common problem is to determine $\hat{\rho}$ on the basis of the system Hamiltonian $\hat{H}_S$ in combination with the bath properties and the specific microscopic coupling mechanism.

In order to evaluate $\hat{\rho}$, the coupling to the baths can be treated perturbatively and a large variety of different approaches have been suggested. For more recent examples, see Refs. [13–19] and references cited therein. Starting with the unmanageable von Neumann equation of the density operator for the full system, a common strategy is to obtain a similar first-order differential equation for $\hat{\rho}$, which is local in time. In the basis of the eigenstates $|a\rangle$ for the system Hamiltonian $\hat{H}_S$ with energies E_a, this equation in general reads as

$$\frac{\partial}{\partial t}\rho_{ab} = i(E_b - E_a)\rho_{ab} + i\langle a|[\hat{\rho}, \hat{H}_{\rm ext}(t)]|b\rangle - \sum_{cd} K_{abcd}\rho_{cd}, \qquad (1)$$

where $\hat{H}_{\rm ext}(t)$ describes possible external excitations of the system by time-dependent fields. We note that our units are $\hbar = 1$, $k_B = 1$, $|e| = 1$ except in Secs. IV, V, and Appendices D and E. Standard perturbation theory in the system-bath couplings provides the Wangsness-Bloch-Redfield (WBR) equations [20,21], and K_{abcd} becomes the Redfield tensor $K^{\rm Red}_{abcd}$. However, the WBR equations do not guarantee the positivity of probabilities, which is clearly an unphysical feature albeit other quantities such as total currents (see Refs. [22,23]) are often well recovered. In fact, only a special class of first-order differential equations specified by Lindblad [24] and Gorini *et al.* [25] guarantees the positivity of $\hat{\rho}$. The most general differential equation for the reduced density operator, which is local in time and which conserves positivity, is given by (see, e.g., Chap. 3.2.2 of Ref. [26])

$$\frac{\partial}{\partial t}\hat{\rho} = i[\hat{\rho}, \hat{H}_{\rm eff}] + \sum_j \Gamma_j\left(\hat{L}_j\hat{\rho}\hat{L}_j^\dagger - \frac{1}{2}\hat{\rho}\hat{L}_j^\dagger\hat{L}_j - \frac{1}{2}\hat{L}_j^\dagger\hat{L}_j\hat{\rho}\right). \qquad (2)$$

Here, $\hat{H}_{\rm eff}(t)$ contains the Hamiltonian $\hat{H}_S + \hat{H}_{\rm ext}(t)$ as well as possible renormalization terms from the couplings to the baths. The dimensionless jump operators $\hat{L}_j$ can be chosen without further restrictions within the Hilbert space of the system and Γ_j is a real number with dimension of energy.[1] For the basis of eigenstates, this provides a corresponding tensor K_{abcd} in Eq. (1), which has special properties as discussed in Ref. [27].

Removing all terms from the Redfield tensor $K^{\rm Red}_{abcd}$ where $E_b - E_a \neq E_d - E_c$, which is called secular approximation (sometimes also rotating wave approximation), renders a Lindblad-type tensor $K^{\rm Sec}_{abcd}$ together with renormalization terms in $\hat{H}_{\rm eff}(t)$ [26]. However, in this case the coherences ρ_{ab} for nondegenerate levels just decay (if they are not driven

*Present address: Institute for Quantum Electronics, ETH Zürich, Auguste-Piccard-Hof 1, 8093 Zürich, Switzerland.

[1]There are different ways to write Eq. (2). For example, Γ_j can be incorporated into $\hat{L}_j$.

externally), while the populations $P_a = \rho_{aa}$ of the states are solely determined by a Pauli master equation

$$\frac{\partial}{\partial t} P_a = \sum_c (R_{c\to a} P_c - R_{a\to c} P_a), \tag{3}$$

with the transition rates $R_{c\to a}$. This excludes the description of a rich field of physics where coherences are actually generated by the bath couplings. This is relevant for, e.g., exciton kinetics [27], resonant tunneling in heterostructures [28,29], and carrier capture [30]. Thus, establishing a Lindblad master equation, where coherences are fully taken into account beyond the secular approximation, is a matter of high interest and several proposals have been made recently [16,27,31,32].

In this paper, we suggest a scheme based on a phenomenological approach, where we require that the jump operators carry information on both the spatial and energetic properties of the jump processes. This position and energy resolving Lindblad (PERLind) approach is straightforward to implement and we demonstrate its versatility to a wide range of systems covering basic transport physics, chemistry, and device technology.

The paper is organized as follows: In Sec. II we specify our PERLind approach, which is based on a heuristic argument. This section is the core of our paper, while the subsequent sections demonstrate three applications of the PERLind approach in different fields of physics, chemistry, and technology. Depending on the interest of the reader, they can be read independently of each other and highlight different technical aspects of the approach. In Sec. III we consider tunneling through a quantum-dot system, where we compare the PERLind approach with exact results and other common approximations such as the Pauli master equation and Redfield kinetics. Moreover, we address the approximate fulfillment of the Onsager relation here. Section IV discusses energy transfer in chromophores in direct comparison with a different approach [27] addressing the same problem. The application of the PERLind approach to quantitative simulations of quantum cascade lasers is addressed in Sec. V, where it actually provides the same type of equations as suggested in Ref. [33]. Several technical details including the relaxation to thermal equilibrium are provided in the appendices.

II. DEFINING THE POSITION AND ENERGY RESOLVING LINDBLAD APPROACH

The background for the approach is a general physical problem in the description of interactions with the bath as sketched in Fig. 1. In many cases, this interaction requires both information on spatial and energetic properties of the system. For example, in quantum-dot systems electrons tunnel from a lead into the region of the dot, which is adjacent to the lead. At the same time, the lead only offers electrons with energies up to its electrochemical potential. This energy information is contained in the eigenstates $\phi_a(\mathbf{r})$ of the dot, which are, however, often extended. These two demands imply an inherent conflict: If the tunneling process is modeled by a jump operator creating $\phi_a(\mathbf{r})$, the new electron would be observable at quite a distance immediately, which can lead to inconsistencies. On the other hand, if the jump operator creates a quantum state of the dot localized close to the lead, it is not clear which energy should be used in the occupation function for the lead electrons.

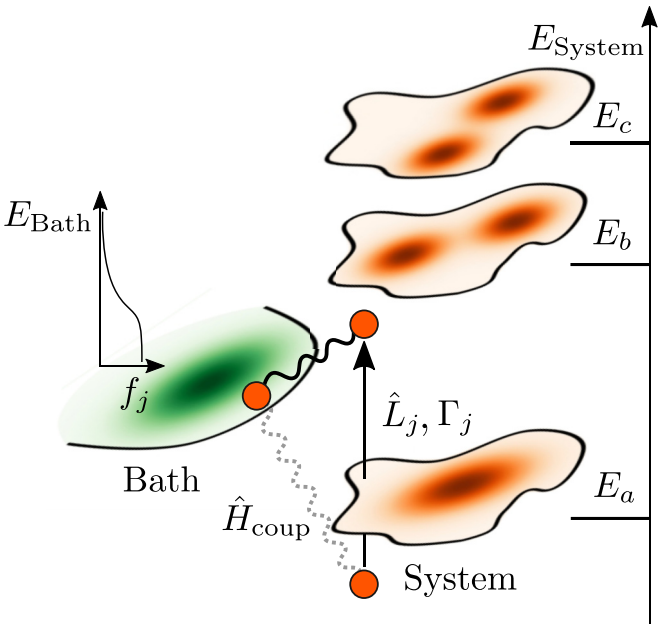

FIG. 1. Scheme of the general problem addressed: The coupling to the bath (left) affects the quantum kinetics in a system (right), where three different energy eigenstates with energies E_a, E_b, and E_c, are depicted. Due to the spatial location of the bath, the transitions by the jump operator $\hat{L}_j$ occur in a particular region of the system as visualized by the vertical arrow. On the other hand, the transition strength depends on the spectral properties of the bath coupling $f_j(E)$, which requires energy information of the system states.

The same holds for vibrations of individual chromophores, which dominantly couple to the local excitations. However, due to excitonic coupling the energy eigenstates are delocalized over several molecules. Again, the bath interaction requires information on spatial and energetic (to match the vibrational frequencies) properties of the quantum states.

Our phenomenological PERLind approach is based on the concept of associating the general jump operators $\hat{L}_j$ in Eq. (2) with specific physical processes due to the bath coupling. Here, the following general procedure is proposed to include both information on locality and the energy spectrum of the bath into the jump operators:

(1) Identify the relevant transitions (numbered by j) in the system due to the bath coupling and quantify them by (i) a dimensionless operator $\hat{L}_j$ specifying the change in the system and taking into account the spatial structure of the bath interaction; (ii) a real dimensionless energy-dependent function $f_j(E)$, where E is the energy the system receives from the bath (this contains the Fermi-Dirac or Bose-Einstein distribution for the bath excitations as well as further spectral properties); and (iii) a prefactor Γ_j, so that $R^j_{\mathrm{i}\to\mathrm{f}} = \Gamma_j f_j(E_\mathrm{f} - E_\mathrm{i}) |\langle \mathrm{f}|\hat{L}_j|\mathrm{i}\rangle|^2$ is the transition rate between the initial state $|\mathrm{i}\rangle$ to the final state $|\mathrm{f}\rangle$. Here, $R^j_{\mathrm{i}\to\mathrm{f}}$ is evaluated by Fermi's golden rule from the microscopic bath coupling $\hat{H}_{\mathrm{coup}}$, where $E_\mathrm{f} - E_\mathrm{i}$ is the energy transfer appearing in the energy balance.

(2) Determine a basis of energy eigenstates of the system $|a\rangle$, $|b\rangle$, etc.

(3) Represent the operators $\hat{L}_j$ in this basis $L^j_{ab} = \langle a|\hat{L}_j|b\rangle$. For particle exchange with leads, $|a\rangle$ and $|b\rangle$ have different particle numbers.

(4) Define $\tilde{L}^j_{ab} = L^j_{ab}\sqrt{f_j(E_a - E_b)}$ and use the Lindblad equation

$$\frac{\partial}{\partial t}\rho_{ab} = i\langle a|[\hat{\rho}, \hat{H}_{\rm eff}(t)]|b\rangle + \sum_{j,cd}\Gamma_j\Big(\tilde{L}^j_{ac}\rho_{cd}\tilde{L}^{j*}_{bd} - \frac{1}{2}\rho_{ac}\tilde{L}^{j*}_{dc}\tilde{L}^j_{db} - \frac{1}{2}\tilde{L}^{j*}_{ca}\tilde{L}^j_{cd}\rho_{db}\Big). \tag{4}$$

This procedure defines an approach for the kinetics of quantum systems in contact with an environment. The presence of $\hat{H}_{\rm eff}(t)$ allows for the inclusion of renormalization effects similar to the secular approximation [26]. However, we do not utilize this feature here.

In this context, it is crucial to note that the energy information $f_j(E)$ is included *on the basis of the matrix elements* for the jump operators. If these operators are not dyadic products of energy eigenstates, this differs essentially from conventional approaches where $\hat{L}_j$ is defined in the form $\sqrt{f_j(E_b - E_a)}|\Psi_b\rangle\langle\Psi_a|$ (see, e.g., Ref. [34]). As explained above, these conventional approaches provide jumps towards energy eigenstates, which do not reflect the spatial properties of the bath coupling.

Within the first step, the identification of jump operators can be tricky, if the same bath couples to different transitions in the system. This can be either understood as different jump processes for each transition or a combined one, where all transitions are subsumed in one operator $\hat{L}_j$. For several situations, we found that the result depends upon this choice: an example is given in Sec. III. Here, we find consistent results, if all transitions connected to identical degrees of freedom in the bath are grouped to a single jump operator $\hat{L}_j$.

We note that our Eq. (4) has the form of Eq. (1) with the tensor

$$K^{\rm PERLind}_{abcd} = -\sum_j\Gamma_j\Big(\tilde{L}^j_{ac}\tilde{L}^{j*}_{bd} - \frac{1}{2}\sum_e\tilde{L}^{j*}_{ed}\tilde{L}^j_{eb}\delta_{ac} - \frac{1}{2}\sum_e\tilde{L}^{j*}_{ea}\tilde{L}^j_{ec}\delta_{bd}\Big). \tag{5}$$

By construction, we find

$$K^{\rm PERLind}_{aacc} = -\sum_j\Big(R^j_{c\to a} - \sum_e R^j_{a\to e}\delta_{ac}\Big),$$
$$K^{\rm PERLind}_{abab} = -\sum_j\Big(\Gamma_j\tilde{L}^j_{aa}\tilde{L}^{j*}_{bb} - \frac{1}{2}\sum_e\big[R^j_{b\to e} + R^j_{a\to e}\big]\Big), \tag{6}$$

which are just the terms of the secular approximation for the Redfield tensor. This shows, that our PERLind approach is an extension of the well-established secular approximation, which is complemented by further elements in $K^{\rm PERLind}_{abcd}$ with $E_b - E_a \neq E_d - E_c$. We note that the imaginary part of $K^{\rm Red}_{abab}$ contributes to $\hat{H}_{\rm eff}$ as a renormalization of the energies $E_b - E_a \to E_b - E_a - {\rm Im}(K^{\rm Red}_{abab})$, however, we do not consider such terms in our approach.

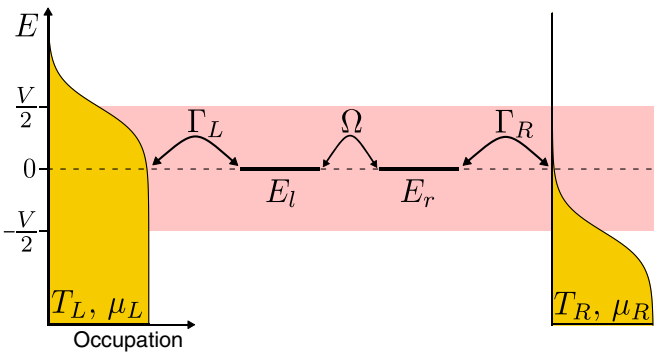

FIG. 2. A simple spin-polarized double-dot structure used to practically demonstrate the PERLind approach. The energy of the dot states is shifted by a gate voltage $V_g = E_l = E_r$. Both dots are coupled to each other (Ω) and to one lead each (Γ_L and Γ_R). The two leads are described as electron reservoirs with applied bias $V = \mu_L - \mu_R$, which results in a particle current I and an energy current $\dot{E}$.

Finally, we consider the equilibration of the system in the limit of weak system-bath coupling. If all baths have the same temperature (and chemical potential for particle exchange), we expect that the density matrix relaxes to its equilibrium value for $\hat{H}_{\rm ext}(t) = 0$. In Appendix A we show that this is indeed the case for our approach in the limit of small system-bath coupling.

III. APPLICATION 1: SPIN-POLARIZED DOUBLE-DOT STRUCTURE

To demonstrate our proposed PERLind scheme, we consider a system of two coupled quantum dots, where each dot has a single spin-polarized energy level (indices l and r). Both dots are coupled to each other and to source (L) and drain (R) leads as depicted in Fig. 2. We have the total Hamiltonian [35–38] $\hat{H}_S + \hat{H}_{\rm leads} + \hat{H}_{\rm coup}$ with the terms

$$\hat{H}_S = V_g\,(\hat{d}^\dagger_l\hat{d}_l + \hat{d}^\dagger_r\hat{d}_r) - \Omega\,(\hat{d}^\dagger_l\hat{d}_r + \hat{d}^\dagger_r\hat{d}_l) + U\,\hat{d}^\dagger_l\hat{d}_l\,\hat{d}^\dagger_r\hat{d}_r, \tag{7a}$$
$$\hat{H}_{\rm leads} = \sum_{\ell k}E_{\ell k}\,\hat{c}^\dagger_{\ell k}\hat{c}_{\ell k}, \tag{7b}$$
$$\hat{H}_{\rm coup} = \sum_k(t_L\hat{d}^\dagger_l\hat{c}_{Lk} + t_R\hat{d}^\dagger_r\hat{c}_{Rk}) + {\rm H.c.} \tag{7c}$$

Here, $\hat{c}^\dagger_{\ell k}$ creates an electron with quantum numbers k in the lead $\ell \in \{L,R\}$ and $\hat{d}^\dagger_i$ creates an electron in the dot $i \in \{l,r\}$. The coupling between left dot (l) and right dot (r) is given by the hybridization Ω and the level energies are given by E_l and E_r. We assume that the level energies are in resonance and controlled by the gate voltage $V_g = E_l = E_r$. Additionally, there can be a charging energy U when both dots are occupied. The energy dispersion in the leads is given by $E_{\ell k}$ and the electrons can tunnel between dots and leads with tunneling amplitudes t_L and t_R. The coupling to the leads is quantified by the transition rates $\Gamma_\ell = 2\pi\sum_k|t_\ell|^2\,\delta(E - E_{\ell k})$, which are assumed to be independent of the energy E

(so-called wide-band limit). We also assume that the leads are in thermal equilibrium and electron occupation is described by a Fermi-Dirac occupation function $f_\ell^{\mathrm{FD}}(E) = [e^{(E-\mu_\ell)/T_\ell} + 1]^{-1}$, where a bias $V = \mu_L - \mu_R$ is applied.

Now, we describe the kinetics of the reduced density matrix of the double-dot using the four steps defined in Sec. II:

(1) There are four different tunneling processes from the leads to the dots:

I. An electron enters from the left lead into the left dot: $\hat{L}_{\mathrm{I}} = \hat{d}_l^\dagger$, $f_{\mathrm{I}}(E) = f_L^{\mathrm{FD}}(E)$, $\Gamma_{\mathrm{I}} = \Gamma_L$.

II. An electron leaves the left dot into the left lead: $\hat{L}_{\mathrm{II}} = \hat{d}_l$, $f_{\mathrm{II}}(E) = 1 - f_L^{\mathrm{FD}}(E)$, $\Gamma_{\mathrm{II}} = \Gamma_L$.

III. An electron enters from the right lead into the right dot: $\hat{L}_{\mathrm{III}} = \hat{d}_r^\dagger$, $f_{\mathrm{III}}(E) = f_R^{\mathrm{FD}}(E)$, $\Gamma_{\mathrm{III}} = \Gamma_R$.

IV. An electron leaves the right dot into the right lead: $\hat{L}_{\mathrm{IV}} = \hat{d}_r$, $f_{\mathrm{IV}}(E) = 1 - f_R^{\mathrm{FD}}(E)$, $\Gamma_{\mathrm{IV}} = \Gamma_R$.

(2) The system Hamiltonian H_S [Eq. (7a)] has four many-particle eigenstates:

$$|0\rangle, \qquad E_0 = 0, \tag{8a}$$

$$|1\rangle = \hat{d}_1^\dagger|0\rangle, \quad E_1 = V_g - \Omega, \tag{8b}$$

$$|1'\rangle = \hat{d}_{1'}^\dagger|0\rangle, \quad E_{1'} = V_g + \Omega, \tag{8c}$$

$$|2\rangle = \hat{d}_{1'}^\dagger\hat{d}_1^\dagger|0\rangle, \quad E_2 = 2V_g + U, \tag{8d}$$

where

$$\hat{d}_1 = \frac{1}{\sqrt{2}}(\hat{d}_l + \hat{d}_r) \quad \text{and} \quad \hat{d}_{1'} = \frac{1}{\sqrt{2}}(\hat{d}_l - \hat{d}_r). \tag{9}$$

(3) In the basis Eq. (8) the jump operators $\hat{L}_j$ are

$$L_{\mathrm{I}} = \frac{1}{\sqrt{2}}\begin{pmatrix} 0 & 0 & 0 & 0 \\ +1 & 0 & 0 & 0 \\ +1 & 0 & 0 & 0 \\ 0 & +1 & -1 & 0 \end{pmatrix}, \quad L_{\mathrm{II}} = (L_{\mathrm{I}})^T,$$

$$L_{\mathrm{III}} = \frac{1}{\sqrt{2}}\begin{pmatrix} 0 & 0 & 0 & 0 \\ +1 & 0 & 0 & 0 \\ -1 & 0 & 0 & 0 \\ 0 & -1 & -1 & 0 \end{pmatrix}, \quad L_{\mathrm{IV}} = (L_{\mathrm{III}})^T.$$

(4) The jump operators $\hat{L}_j$ are weighted by $\sqrt{f_j(E)}$ to give $\tilde{L}_{ab}^j = L_{ab}^j\sqrt{f_j(E_a - E_b)}$. Thus,

$$2\tilde{L}_{\mathrm{I}} = \frac{1}{\sqrt{2}}\begin{pmatrix} 0 & 0 & 0 & 0 \\ \sqrt{f_L^{\mathrm{FD}}(V_g - \Omega)} & 0 & 0 & 0 \\ \sqrt{f_L^{\mathrm{FD}}(V_g + \Omega)} & 0 & 0 & 0 \\ 0 & \sqrt{f_L^{\mathrm{FD}}(V_g + \Omega + U)} & -\sqrt{f_L^{\mathrm{FD}}(V_g - \Omega + U)} & 0 \end{pmatrix},$$

$$\tilde{L}_{\mathrm{III}} = \frac{1}{\sqrt{2}}\begin{pmatrix} 0 & 0 & 0 & 0 \\ \sqrt{f_R^{\mathrm{FD}}(V_g - \Omega)} & 0 & 0 & 0 \\ -\sqrt{f_R^{\mathrm{FD}}(V_g + \Omega)} & 0 & 0 & 0 \\ 0 & -\sqrt{f_R^{\mathrm{FD}}(V_g + \Omega + U)} & -\sqrt{f_R^{\mathrm{FD}}(V_g - \Omega + U)} & 0 \end{pmatrix},$$

and $\tilde{L}_{\mathrm{II}}$ ($\tilde{L}_{\mathrm{IV}}$) is obtained by transposing $\tilde{L}_{\mathrm{I}}$ ($\tilde{L}_{\mathrm{III}}$) and by replacing f_ℓ^{FD} with $1 - f_\ell^{\mathrm{FD}}$.

After inserting Γ_j and $\tilde{L}_j$ into Eq. (4), we obtain a master equation for the reduced density matrix. In the long-time limit, a stationary state is reached, which we determine directly by setting $\partial_t\rho_{ab} = 0$ in Eq. (4). For this stationary state we can calculate various observables. In particular, we are interested in the particle (I_L) and energy ($\dot{E}_L$, as relevant for thermoelectric applications [39]) currents flowing from the left lead into the system, which are calculated by

$$I_L = \sum_{baa'}\left(\Gamma_{\mathrm{I}}\tilde{L}_{ba}^{\mathrm{I}}\rho_{aa'}\tilde{L}_{ba'}^{\mathrm{I}*} - \Gamma_{\mathrm{II}}\tilde{L}_{ba}^{\mathrm{II}}\rho_{aa'}\tilde{L}_{ba'}^{\mathrm{II}*}\right), \tag{10}$$

$$\dot{E}_L = \sum_{\substack{j=\mathrm{I,II} \\ baa'}}\Gamma_j\left(E_b - \frac{E_a + E_{a'}}{2}\right)\tilde{L}_{ba}^j\rho_{aa'}\tilde{L}_{ba'}^{j*}. \tag{11}$$

See Appendix B for the definition and more details on the particle current and energy current observables.

We focus on the noninteracting case $U = 0$, where the transmission formalism [40–42] provides an exact solution (see Appendix C 1). The analytic solution of the resulting master equation for the reduced density matrix using the PERLind approach in the noninteracting case $U = 0$ is discussed in Appendix C 2.

The results for symmetric coupling $\Gamma_L = \Gamma_R = \Gamma$ are shown in Fig. 3. At first, we see that the result of the PERLind scheme is very close to the transmission result. The main difference is that the current peaks are slightly lower and broader in the transmission calculation, which includes tunneling to all orders and thus takes level broadening into account. This difference vanishes with increasing temperature, while for $T < \Gamma$ the discrepancy becomes more substantial. We also display the result for the Redfield equations, which can be directly applied to tunneling systems [43] (see Appendix C 3 for more details). This approach works reasonably well, but agrees less with the correct transmission result than our suggested approach. It is interesting to note that neglecting the principal value integrals (Redfield, no $\mathcal{P}$) provides slightly

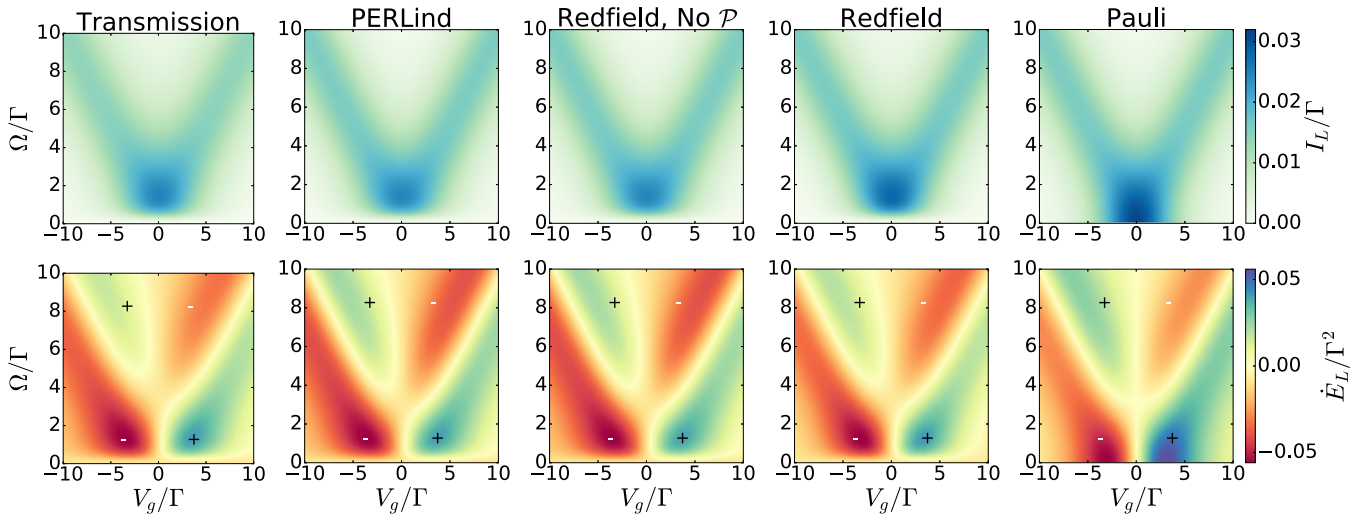

FIG. 3. Simulations of the noninteracting double-dot system using different approaches for equal energies $E_1 = E_2$ and symmetric coupling $\Gamma_L = \Gamma_R = \Gamma$. Other parameters are $\mu_L = -\mu_R = \Gamma/4$ and $T = 2\Gamma$. The $+/-$ signs indicate the sign of the energy current.

better results for the used parameters. Finally, we observe that the Pauli master equation, which has the same stationary state as the secular approximation, fails for small interdot coupling $\Omega \to 0$. Here, the current remains finite, which is an artifact of the neglect of coherences in the basis of eigenstates. The electrons from the left lead enter one of the eigenstates, which are distributed over both dots and are allowed to leave to the right lead immediately. Thus, the current is solely determined by Γ in this case. This issue is well known and appears in many circumstances [29,44,45]. It is clear that the proposed PERLind approach correctly treats this problem. Compared to the Redfield approach, it provides results even closer to the exact solution and, most importantly, avoids negative probabilities. Lastly, we note that the simulations of the double-dot structure using PERLind, Redfield, and Pauli approaches were produced with the QMEQ package [46] using the `kerntype` options `Lindblad`, `Redfield`, and `Pauli`, respectively. This publicly available package allows to perform corresponding calculations for more complex systems in a straightforward way.

A. Choice of jump operators

The choice of jump operators, which we made so far, is not a unique one. This can be seen by considering the tunneling Hamiltonian (7c) expressed in the eigenbasis (9):

$$\hat{H}_{\text{coup}} = \sum_k \left[\frac{t_L}{\sqrt{2}} (\hat{d}_1^\dagger + \hat{d}_{1'}^\dagger)\hat{c}_{Lk} + \frac{t_R}{\sqrt{2}} (\hat{d}_1^\dagger - \hat{d}_{1'}^\dagger)\hat{c}_{Rk} \right] + \text{H.c.} \tag{12}$$

We can translate Eq. (12) into jump operators at least in two different ways. Let us consider the jump processes related just to the left lead (right lead is analogous):

(i) We use four jump operators, namely, $\hat{L}_{\text{i}} = \hat{d}_1^\dagger$ and $\hat{L}_{\text{ii}} = \hat{d}_{1'}^\dagger$ for entering the quantum dots from the left lead as well as $\hat{L}_{\text{iii}} = \hat{d}_1$ and $\hat{L}_{\text{iv}} = \hat{d}_{1'}$ for electrons leaving the quantum dots into the left lead.

(ii) We subsume these into two jump operators $\hat{L}_{\text{I}} = \hat{d}_1^\dagger + \hat{d}_{1'}^\dagger$ and $\hat{L}_{\text{III}} = \hat{d}_1 + \hat{d}_{1'}$. This corresponds to the same choice which we did in the beginning of the section.

The choice (i) gives the results of the Pauli master equation for the double-dot structure, where in the stationary state there are no coherences. Thus, the case (ii) should be preferred.

A good argument for the choice (ii) is based on another approach. The left lead provides electrons at a position z_L (e.g., in the barrier between the leftmost dot and the reservoir). Thus, the jump operator is actually the field operator $\hat{\Psi}^\dagger(z_L)$. Expanding in the state of the quantum dot, we obtain $\hat{\Psi}^\dagger(z_L) = \phi_1^*(z_L)\hat{d}_1^\dagger + \phi_{1'}^*(z_L)\hat{d}_{1'}^\dagger$. Assuming an equal coupling strength for both levels in (12) implies $\phi_1(z_L) = \phi_{1'}(z_L)$ and we obtain version (ii) after incorporating $\phi_1(z_L)$ into the tunneling rate Γ.

B. Onsager's relation

It was recently shown that the Redfield approach also predicts charge currents that are not consistent with the exchange fluctuation theorems [47], and that for our considered double-dot structure Onsager relations relating particle current to heat current are not satisfied (for more details, see Ref. [48]). This raises the following question: Does our proposed PERLind scheme satisfy Onsager relations? Thus, we consider the deviation Δ_{O} from the Onsager relation for the particle current I_L and the heat current $Q_L = \dot{E}_L - \mu_L I_L$:

$$\begin{aligned} \Delta_{\text{O}} &= L_1' - L_1 = 0, \\ L_1' &= \left.\frac{\partial Q_L}{\partial V}\right|_{V=0,\Delta T=0}, \\ L_1 &= T \left.\frac{\partial I_L}{\partial \Delta T}\right|_{V=0,\Delta T=0}, \end{aligned} \tag{13}$$

where the bias V and temperature difference ΔT are applied as $\mu_{L/R} = \pm V/2$, $T_{L/R} = T \pm \Delta T/2$. Here, L_1' and L_1 are the Onsager coefficients, which should not be confused with the jump operators. After using analytic expressions for the

currents in Eqs. (C8) and inserting them into relation (13) we obtain for a symmetric coupling $\Gamma_L = \Gamma_R = \Gamma$

$$\Delta_{\rm O} = -\frac{\Gamma^3}{32\widetilde{\Omega}T}(s+\bar{s})(f_+ - f_-) \times[(\bar{f}_+ + \bar{f}_-)s - (f_+ + f_-)\bar{s}] \neq 0, \quad (14)$$

where

$$\widetilde{\Omega} = \Omega(1+\gamma^2), \quad \gamma = \frac{\Gamma}{2\Omega},$$
$$f_\pm = 1/[e^{(V_g \pm \Omega)/T_L} + 1], \quad \bar{f}_\pm = 1 - f_\pm, \quad (15)$$
$$s = \sqrt{f_+ f_-}, \quad \bar{s} = \sqrt{\bar{f}_+ \bar{f}_-}.$$

From Eq. (14) we see that formally the Onsager's relation is not satisfied. However, similarly as in Ref. [48] the violation is of higher order in Γ than the currents, and for sufficiently weak coupling no problem arises. We quantify this violation by considering the ratio of the peak value $\Delta_{\rm O,peak} = \max_{V_g,\Omega}|\Delta_{\rm O,peak}(V_g,\Omega)|$ to the peak value $L_{1,\rm peak} = \max_{V_g,\Omega}|L_1(V_g,\Omega)|$ in the (V_g,Ω) parameter space. For example, when $\Gamma = T/2$ the proposed Lindblad scheme gives $\Delta_{\rm O,peak}/L_{1,\rm peak} \approx 0.4\%$. The corresponding violation ratio for the Redfield approach is 16% and for the no $\mathcal{P}$ approach is 3%, which is higher than for PERLind scheme.

Alicki [49] showed that the Onsager's theorem is satisfied for a system described by Lindblad kinetics if the *quantum detailed balance* condition is fulfilled [50–53]. One of the requirements for this is the commutation relation $[\rho, H_S] = 0$ between the density matrix of the system and the system Hamiltonian [49,54]. For our case this implies that in the stationary state the coherences between nondegenerate states to linear order in V and ΔT have to be equal to zero. This is not the case for our proposed PERLind scheme when applied to the double-dot system, as can be seen from Eq. (C7), so that the *quantum detailed balance* condition is violated. However, as argued above, the nonvanishing coherence is essential to describe the transport in the double dot, as this provides the spatial information for degenerate dot levels $E_r = E_l$. Thus, the violation of quantum detailed balance and Onsager's theorem is the price to pay for establishing a Lindblad-type kinetics, which provides a physically correct result.

C. Asymmetric couplings

Using asymmetric coupling $\Gamma_L = (1+b)\Gamma$, $\Gamma_R = (1-b)\Gamma$ for the two leads, we find that our proposed PERLind scheme provides actually a current flow at zero bias ($V = 0$, $\Delta T = 0$):

$$I_L = -\frac{1}{2}\Gamma\gamma^2 b(1-b^2)(s+\bar{s})\frac{(\bar{f}_+ + \bar{f}_-)s - (f_+ + f_-)\bar{s}}{1+\gamma^2[1-b^2(s+\bar{s})^2]}. \quad (16)$$

As in the case with the violation of Onsager's theorem, this current is of order Γ^3 and thus beyond the relevant perturbation theory. The first-order Redfield approach also suffers from this problem, where the current at zero bias is determined by the principal part $\mathcal{P}$ integrals:

$$I_L^{\rm Red} = -\frac{\Gamma^2 b(1-b^2)}{1+\gamma^2(1-b^2)}\frac{1}{2\pi}\mathcal{P}\int_{-\infty}^{\infty}\frac{dEf(E)}{(E-V_g)^2 - \Omega^2}. \quad (17)$$

Neglecting the principal part integrals, the current becomes zero for the Redfield approach in this particular case.

IV. APPLICATION 2: EXCITON KINETICS IN A SYSTEM OF TWO CHROMOPHORES

Here, we apply the PERLind approach to exciton kinetics. We use the particular example discussed in Ref. [27] where a different way to obtain a Lindblad equation from a Redfield tensor is discussed. For comparison, we show our results for the two two-level chromophore system considered in Ref. [27], which is described by the total Hamiltonian $\hat{H}_S + \hat{H}_{\rm baths} + \hat{H}_{\rm coup}$:

$$\hat{H}_S = E_1\hat{B}_1^\dagger\hat{B}_1 + E_2\hat{B}_2^\dagger\hat{B}_2 + V(\hat{B}_1^\dagger\hat{B}_2 + \hat{B}_2^\dagger\hat{B}_1), \quad (18a)$$
$$\hat{H}_{\rm baths} = \sum_{k,i=1,2} E_k\hat{a}_{ik}^\dagger\hat{a}_{ik}, \quad (18b)$$
$$\hat{H}_{\rm coup} = d_{\rm ph}\sum_{k,i=1,2}\hat{B}_i^\dagger\hat{B}_i(\hat{a}_{ik} + \hat{a}_{ik}^\dagger). \quad (18c)$$

Here, $\hat{B}_i^\dagger$ creates an excitation on chromophore i, which is individually coupled to a local phonon bath. Operator $\hat{a}_{ik}^\dagger$ creates a phonon in a mode k and in a bath i. We note that all operators satisfy canonical commutation relations $[\hat{B}_i, \hat{B}_{i'}^\dagger] = \delta_{ii'}$, $[\hat{a}_{ik}, \hat{a}_{i'k'}^\dagger] = \delta_{ii'}\delta_{kk'}$. The excitation energies are $E_1 = 0$ and $E_2 = 46.4\times hc/\text{cm}$, and the coupling strength between the excitations is $V = -71.3\times hc/\text{cm}$. The modes of the phonon baths have the density of states of overdamped Brownian oscillator [6]

$$\nu(E) = \frac{2\hbar\Lambda|E|}{E^2 + (\hbar\Lambda)^2}\nu_0, \quad (19)$$

where $\Lambda = 1/106$ fs^{-1} is the inverse of the bath correlation time.

The kinetics of the reduced density matrix for the two two-level chromophore system is described using the four steps defined in Sec. II:

(1) There are four different jump processes, which dephase the chromophore excitations, with the same rate $\Gamma = 2\pi\nu_0|d_{\rm ph}|^2 = 2hc\lambda$, where $\lambda = 35$ cm:

I. $\hat{L}_{\rm I} = \hat{B}_1^\dagger\hat{B}_1$, $f_{\rm I}(E) = \frac{\nu(E)}{\nu_0}n(E)\theta(E)$, with $n(E) = 1/[e^{E/(k_{\rm B}T)} - 1]$, where $\theta(E)$ is the Heaviside step function.

II. $\hat{L}_{\rm II} = \hat{B}_1^\dagger\hat{B}_1$, $f_{\rm II}(E) = \frac{\nu(-E)}{\nu_0}[1+n(-E)]\theta(-E)$.

III. $\hat{L}_{\rm III} = \hat{B}_2^\dagger\hat{B}_2$, $f_{\rm III}(E) = \frac{\nu(E)}{\nu_0}n(E)\theta(E)$.

IV. $\hat{L}_{\rm IV} = \hat{B}_2^\dagger\hat{B}_2$, $f_{\rm IV}(E) = \frac{\nu(-E)}{\nu_0}[1+n(-E)]\theta(-E)$.

(2) The chromophore Hamiltonian (18a) has the excitonic eigenstates ($\hat{H}_S = \varepsilon_1\hat{e}_1^\dagger\hat{e}_1 + \varepsilon_2\hat{e}_2^\dagger\hat{e}_2$)

$$\hat{e}_1 = \alpha\hat{B}_1 + \beta\hat{B}_2, \quad \alpha = 0.81$$
$$\hat{e}_2 = \beta\hat{B}_1 - \alpha\hat{B}_2, \quad \beta = 0.59 \quad (20)$$

which are delocalized and which have the eigenenergies $\varepsilon_1 = -51.7\times hc/\text{cm}$ and $\varepsilon_2 = 98.2\times hc/\text{cm}$. We consider the dynamics of a single excitation in the chromophore system with the initial condition $\rho_{11} = \rho_{22} = \rho_{12} = 0.5$ in the basis (20). The Hamiltonian (18) conserves the number of excitations and

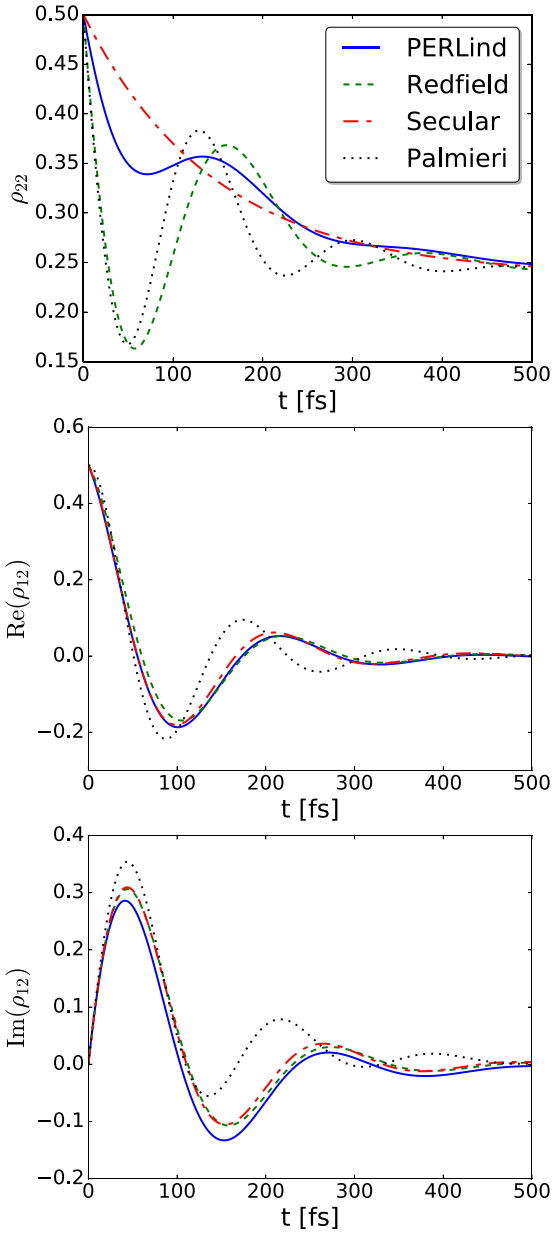

FIG. 4. Results for the system of Ref. [27] at $T = 185$ K and $\lambda = 35$ cm. Full lines depict the results for the density matrix in our model (PERLind). Dashed lines show the Redfield approach, dashed-dotted lines show the secular approximation, and dotted lines show the Lindblad model of Ref. [27] (Palmieri), all without principal value parts. The initial condition is chosen as $\rho_{11} = \rho_{22} = \rho_{12} = 0.5$ in the basis of eigenstates.

there is no coupling between the states with no excitation and two excitations, so it is enough to consider the subspace of a single excitation.

(3) In the basis (20), the jump operators $\hat{L}_j$ are

$$L_{\mathrm{I}} = \begin{pmatrix} \alpha^2 & \alpha\beta \\ \alpha\beta & \beta^2 \end{pmatrix}, \quad L_{\mathrm{II}} = L_{\mathrm{I}},$$

$$L_{\mathrm{III}} = \begin{pmatrix} \beta^2 & -\alpha\beta \\ -\alpha\beta & \alpha^2 \end{pmatrix}, \quad L_{\mathrm{IV}} = L_{\mathrm{III}}. \tag{21}$$

(4) The jump operators L_j are weighted by $\sqrt{f_j(E)}$ to give $\tilde{L}^j_{ab} = L^j_{ab}\sqrt{f_j(E_a - E_b)}$.

This provides the tensor K^{PERLind} given in Eq. (D3). Its secular elements fully agree with the full Redfield tensor given in Eq. (D1).

In Fig. 4 we show the results of our PERLind approach in comparison with the secular approximation and another Lindblad model discussed by Palmieri *et al.* [27]. We find that our approach provides oscillating occupations, which only show a decay in the secular approximation. However, this oscillating feature is weaker compared to the results from the approach suggested in Ref. [27] and the Redfield approach. On the other hand, the coherences obtained from our method are closer to the Redfield approach than the ones obtained by the previous method. As we do not have an exact result to compare with, it is difficult to judge which method is better here.

V. APPLICATION 3: SIMULATION OF QUANTUM CASCADE LASERS

The quantum cascade laser (QCL) [55,56] is an important device for the generation of infrared and terahertz radiation. It is based on optical transitions between quantum states $\psi_\alpha(z)$ with energy E_α in the conduction band of a semiconductor heterostructure (with growth direction z) as depicted in the inset of Fig. 5. The operation relies on an intricate interplay of tunneling and scattering transitions under the applied bias. Laterally, the QCL layers cover an area A, which is assumed to be homogeneous (after impurity averaging) and large compared to the layer thicknesses, so that quantization in the x, y direction (expressed by bold vectors $\mathbf{r}$ in the following) is not relevant. Instead, a quasicontinuum of eigenstates $\frac{1}{\sqrt{A}}e^{i\mathbf{k}\cdot\mathbf{r}}$ with

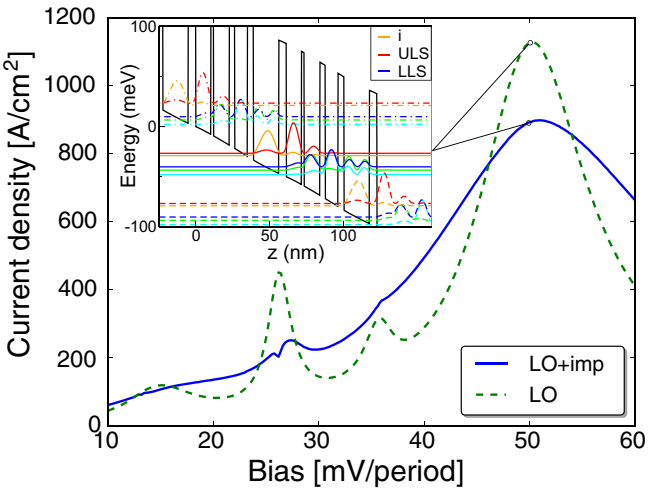

FIG. 5. Current density dependence on bias per period for the QCL of Ref. [72], with LO phonon scattering only (dashed curve), as well as with added impurity scattering (solid curve). The temperature in these simulations is $T = 150$ K. The inset shows the Wannier-Stark levels at a bias of 50 mV/period (marked by circles on the current-bias curves), and the upper laser state (ULS), lower laser state (LLS), and the injector state (i) are indicated. The energy difference is 13.1 meV between the ULS and LLS, and 38.3 meV between the LLS and injector of the next period. The ULS is 1.4 meV above level i.

wave vector $\mathbf{k}$ is assumed, so that the energy of the quantum state $|\alpha,\mathbf{k}\rangle$ is $E_{\alpha\mathbf{k}} = E_\alpha + E_\mathbf{k}$. Here, $E_\mathbf{k} = \hbar^2\mathbf{k}^2/(2m_c)$ with the effective mass m_c of the conduction band. Within this basis, we have the single-particle density matrix

$$\rho_{\beta\alpha}(\mathbf{k}) = \mathrm{Tr}\{\hat{\rho}\hat{c}^\dagger_{\alpha\mathbf{k}}\hat{c}_{\beta\mathbf{k}}\}\,. \tag{22}$$

Its diagonal elements are the occupation probabilities $f_{\alpha\mathbf{k}} = \rho_{\alpha\alpha}(\mathbf{k})$. Of physical interest are the electron densities in the individual levels (taking into account spin degeneracy)

$$n_\alpha = \frac{2}{A}\sum_\mathbf{k} f_{\alpha\mathbf{k}}\,, \tag{23}$$

and the current density

$$J(z) = \frac{-e}{A}\sum_{\mathbf{k},\alpha\beta}\mathrm{Re}\left\{\rho_{\beta\alpha}(\mathbf{k})\psi^*_\alpha(z)\frac{\hbar}{m_c(z)i}\frac{\partial\psi_\beta(z)}{\partial z}\right\}, \tag{24}$$

where $e > 0$ is the elementary charge. Note that both quantities only depend on the average density matrix

$$\rho_{\beta\alpha} = \frac{2}{A}\sum_\mathbf{k}\rho_{\beta\alpha}(\mathbf{k}). \tag{25}$$

In a basis of real wave functions $\psi_\alpha(z)$, such as the commonly used energy eigenfunctions, we find that the current solely depends on the coherences [57]. However, these coherences can be approximated based on occupations [58] allowing simulation schemes restricting to the occupation probabilities $f_{\alpha\mathbf{k}}$ (e.g., Refs. [59,60]) or electron densities n_α (e.g., Ref. [61]). Here, the kinetics is given by scattering rates in the form of the Pauli master equation. This entirely neglects the coherences and consequently fails to describe resonant tunneling correctly [29] similar to the tunneling in the double dot of Sec. III.

Considering coherences within the average density matrix $\rho_{\alpha\beta}$ is frequently done phenomenologically [62–64]. Taking into account the lateral degrees of freedom, more detailed Redfield-type schemes for the simulation of $\rho_{\alpha\beta}(\mathbf{k})$ have been developed [22,23,65,66], which can provide unphysical negative occupations as discussed in Ref. [22]. The common solution is to use Green's function approaches [57,67–70] allowing for a full consistent treatment at the price of a high numerical demand. Here, we show that the PERLind approach provides a viable quantum kinetics for the average density matrix $\rho_{\alpha\beta}$ which is based on the microscopic scattering interaction.

An important scattering mechanism in QCLs is the electron-phonon interaction, which enhances the electron transitions between different subbands. For electron-phonon interaction we use the Hamiltonian [71]

$$\hat{H}_{\text{el-ph}} = \sum_{\substack{\alpha,\beta\\ \mathbf{k},\mathbf{q},q_z}} M^{q_z}_{\beta\alpha} g_{\mathbf{q},q_z}\hat{c}^\dagger_{\beta,\mathbf{k}+\mathbf{q}}\hat{c}_{\alpha,\mathbf{k}}\hat{b}_{\mathbf{q},q_z} + \text{H.c.}, \tag{26}$$

where $\mathbf{q}$ and q_z are the in-plane and z components of the phonon wave vector and $\hat{b}_{\mathbf{q},q_z}$ are the bosonic phonon operators. Furthermore, we define

$$M^{q_z}_{\beta\alpha} = \int dz\,\psi^*_\beta(z)e^{iq_z z}\psi_\alpha(z)\,. \tag{27}$$

Within Fermi's golden rule this provides the scattering rates between the states in the heterostructure

$$\Gamma_{\alpha\mathbf{k}\to\beta\mathbf{k}'} = \frac{2\pi}{\hbar}\sum_{q_z}\left|M^{q_z}_{\beta\alpha}\right|^2\Big[\left|g_{\mathbf{k}'-\mathbf{k},q_z}\right|^2\delta(E_{\beta\mathbf{k}'} - E_{\alpha\mathbf{k}} + \hbar\omega_{\text{LO}}) \times [f_B(\hbar\omega_{\text{LO}}) + 1] + \left|g_{\mathbf{k}-\mathbf{k}',-q_z}\right|^2\delta(E_{\beta\mathbf{k}'} - E_{\alpha\mathbf{k}} - \hbar\omega_{\text{LO}})f_B(\hbar\omega_{\text{LO}})\Big] \tag{28}$$

for dispersionless phonons with frequency ω_{LO}. Here, $f_B(E)$ is the Bose distribution, assuming that the phonons are in thermal equilibrium at the simulation temperature T. The average transition rate for all lateral states is then given by

$$R_{\alpha\to\beta} = \frac{\sum_{\mathbf{k},\mathbf{k}'} f_{\alpha,\mathbf{k}}\Gamma_{\alpha\mathbf{k}\to\beta\mathbf{k}'}}{\sum_\mathbf{k} f_{\alpha,\mathbf{k}}}. \tag{29}$$

Assuming that $f_{\alpha,\mathbf{k}}$ is a thermal distribution, this can be cast into the form

$$R_{\alpha\to\beta} = \sum_{q_z}\left|M^{q_z}_{\beta\alpha}\right|^2 f_{q_z}(E_\beta - E_\alpha). \tag{30}$$

Details are given in Appendix E 1 for polar optical phonon scattering. We note that $M^{q_z}_{\beta\alpha}$ takes into account the spatial overlap of the states in connection with the perturbation potential, while $f_{q_z}(E_\beta - E_\alpha)$ solely depends on the energy. This is just the form assumed in step 1 of our general approach: here, we identify $M^{q_z}_{\beta\alpha}$ with $\langle\psi_\beta|\hat{L}_{q_z}|\psi_\alpha\rangle$ and $f_{q_z}(E_\beta - E_\alpha)$ is just the distribution function, where we set $\Gamma_{q_z} = 1$. Defining $\tilde{L}^{q_z}_{\beta\alpha} = \sqrt{f_{q_z}(E_\beta - E_\alpha)}M^{q_z}_{\beta\alpha}$, we thus obtain the PERLind master equation (4). The tensor (5) obtained in this way has the same structure as Eqs. (19) and (20) of Ref. [33], where a slightly different notation and index labeling is used. Going beyond these results, we also add impurity scattering in the same way (see Appendix E 2).

We will now use this formalism to show that it can accurately simulate QCLs. Specifically, we consider the QCL design published by Li *et al.* [72] and provide a quantitative comparison with experimental data. This design has a periodic sequence of 180 modules, each consisting of four $Al_{0.16}Ga_{0.84}As$ barriers and four GaAs wells (see the inset of Fig. 5). As this requires far too many states to simulate, we consider three modules together with periodic boundary conditions, i.e., assuming that the density matrix is identical, when shifting all states by one period. The states $\psi_\alpha(z)$ are the energy eigenstates which are determined following the procedure of Ref. [73] and we use the five lowest states per module (see the inset of Fig. 5), which amounts to 15 states in total. For our periodic conditions, the density matrix takes into account coherences within all the states in these three central modules as well as with the three neighboring modules on either side. Note that the calculations are based on the nominal experimental sample parameters and standard semiconductor material parameters. There is no kind of fitting.

The current density through the QCL is evaluated from Eq. (24) by using $\rho^s_{\alpha\beta} = \rho_{\alpha\beta}(+\infty)$ obtained from stationary PERLind equations. Also, we average $J(z)$ over one module

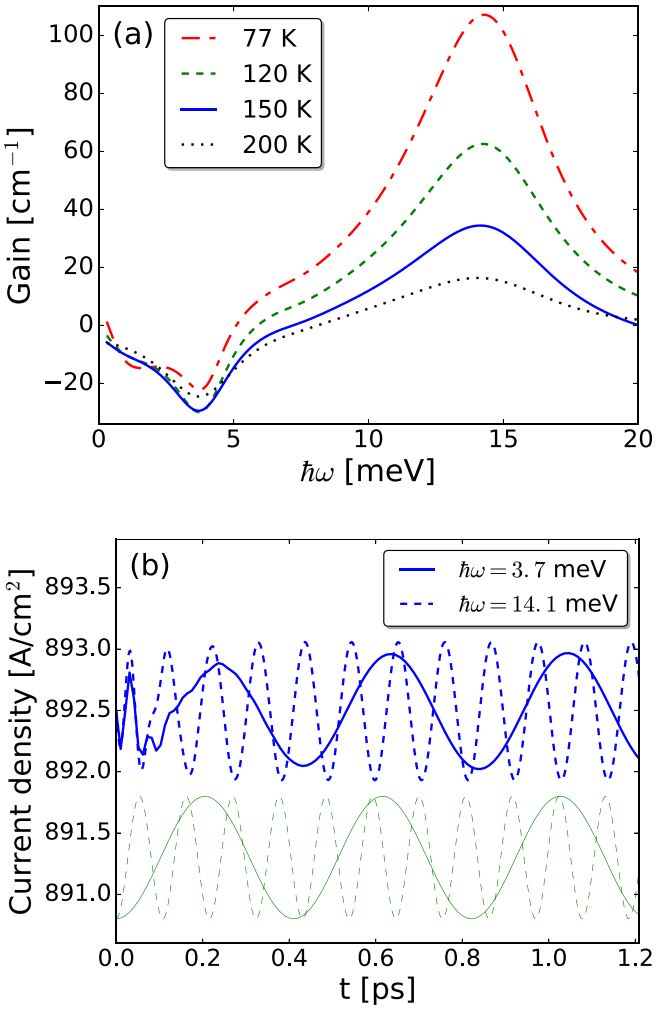

FIG. 6. (a) Calculated gain spectrum for different simulation temperatures for the QCL design of Ref. [72] at 50 mV/period bias. (b) Time-resolved current density at $T = 150$ K (blue thick curves) and electric field (green thin curves with oscillation amplitude $eF_{ac}d = 0.01$ meV) at the points of maximum absorption ($\hbar\omega = 3.7$ meV) and gain ($\hbar\omega = 14.1$ meV), where the current density is in and out of phase with the electric field after a transient phase, respectively.

in order to compensate for spatial variations due to the finite number of basis states. The resulting current-bias relation is shown in Fig. 5. Taking only into account optical phonon scattering, we find several sharp current peaks, similar to Ref. [33]. Adding impurity scattering, these peaks are smeared out and we observe a current peak of about 900 A/cm^2 in accordance with experimental observations [72]. At this operation point, the injector level is aligned with the upper laser level, resulting in efficient tunneling as shown in the inset.

At a bias of 50 mV per module we observe population inversion between the upper and lower laser states. In order to determine the optical gain, we include the optical field [with electrical field strength $F(t) = F_{\rm ac}\cos(\omega t)$ and frequency $\omega/2\pi$] in the model via

$$\hat{H}_{\rm ext}(t) = eF_{\rm ac}\hat{z}\cos(\omega t). \tag{31}$$

For gain simulations, we evolve the PERLind equations in time, taking the stationary density matrix as an initial condition $\rho(0) = \rho^s$. The field generates an alternating current $J(t) \approx J_{\rm dc} + J_{\cos}\cos(\omega t) + J_{\sin}\sin(\omega t)$ (after a transient phase) as depicted in Fig. 6(b). The ratio between induced current and ac field provides the optical gain [70] by $-J_{\cos}/(F_{\rm ac}\sqrt{\epsilon_r}\epsilon_0 c)$. This gain is positive, if $J(t)$ and $F(t)$ are out of phase, and conversely loss prevails when they are in phase. Figure 6(a) shows the resulting gain spectra for different simulation temperatures. We find a pronounced gain peak at 14 meV, i.e., 3.4 THz, which exactly matches the experimental value [72]. The photon energy slightly surpasses the separation between the upper and lower laser levels (13.1 meV), which indicates possible transitions to levels slightly below the LLS. The gain strongly drops with temperature. For surface-plasmon waveguides, the threshold requires gain of the order of 30–40 cm [74], which is achieved for simulation temperatures below 150 K. Experimentally, lasing was observed for heat sink temperatures up to 123 K, which is in good accordance with our simulations. Here, we note in passing that the simulation temperature should be several tens of degrees warmer than the heat sink temperature due to nonequilibrium distributions of optical phonons and electrons [75–77], which we did not quantify here.

Thus, the PERLind approach allows for realistic simulations of QCLs both with respect to steady-state transport and gain. Furthermore, the PERLind approach can also be applied to arbitrary pulses in the optical field and multimode harmonic fields containing an arbitrary number of frequency components, which allows for a variety of interesting applications.

VI. CONCLUSION

We proposed the position and energy resolving Lindblad (PERLind) approach for simulation of open quantum systems by constructing jump operators with a specified energy and spatial dependence. This approach combines the treatment of coherences on a microscopic basis, such as in the Redfield kinetics, with keeping the positivity of the diagonal elements of the density matrix. It can be easily applied to a large variety of different physical systems, where we gave specific examples for tunneling through quantum-dot systems, exciton kinetics in chromophores, and the simulation of quantum cascade lasers. Comparison with the exact solution for tunneling through a double dot and experimental data of a quantum cascade laser verifies the accuracy of the approach. On the other hand, one has to keep in mind that the coupling to the bath is of perturbative nature and the projection of the system dynamics to a time-local Lindblad equation beyond secular approximation can violate general conditions. As an example, PERLind may violate the Onsager relations for strong bath couplings. This appears to be the price to pay for obtaining manageable equations for a simple description of realistic quantum systems with many degrees of freedom, where the coherences in the steady state are crucial.

ACKNOWLEDGMENTS

We thank V. Trinité, P. Hofer, and M. Hell for discussions. Financial support from the Swedish Science Council

(Vetenskapsrådet, Grant No. 621-2012-4024), NanoLund, as well as the Knut and Alice Wallenberg foundation are gratefully acknowledged. The figures were produced using MATPLOTLIB [78].

APPENDIX A: EQUILIBRIUM

Here, we investigate whether thermal equilibrium $\rho^0_{ab} = \delta_{ab}\exp(\beta\mu N_a - \beta E_a)/Z$ provides a stationary solution, when all reservoirs are Bose/Fermi functions with chemical potential μ and inverse temperature $\beta = 1/T$ and $\hat{H}_{\rm eff}(t)$ is time independent and diagonalized with the states $|a\rangle, |b\rangle$, etc. We define $\rho_{ab} = \rho^0_{ab} + \delta\rho_{ab}$ and find from Eq. (4)

$$\frac{\partial}{\partial t}\delta\rho_{ba} = i(E_a - E_b)\delta\rho_{ba} + \sum_{j,c}\Gamma_j\Big(\tilde{L}^j_{ac}\rho^0_{cc}\tilde{L}^{j*}_{bc} - \frac{1}{2}\rho^0_{aa}\tilde{L}^{j*}_{ca}\tilde{L}^j_{cb} - \frac{1}{2}\tilde{L}^{j*}_{ca}\tilde{L}^j_{cb}\rho^0_{bb}\Big) + \mathcal{O}\{\Gamma\delta\rho\}. \quad \text{(A1)}$$

Due to the Hermiticity of the microscopic bath couplings [see, e.g., Eq. (7c)], we find that for any matrix element $\tilde{L}^j_{ba}$, there is a unique corresponding one with $\tilde{L}^{j'}_{ab} = \tilde{L}^{j*}_{ba}e^{\beta(E_b-E_a)/2-\beta\mu(N_b-N_a)/2}$. Here, j and j' may result from different jump processes, such as adding or removing a particle. We also have $\rho^0_{bb} = \rho^0_{aa}e^{\beta\mu(N_b-N_a)-\beta(E_b-E_a)}$. Renaming $j \to j'$ for the terms with $\frac{1}{2}$ we obtain

$$\frac{\partial}{\partial t}\delta\rho_{ba} = i(E_a - E_b)\delta\rho_{ba} + \sum_{j,c}\Gamma_j\rho^0_{cc}\tilde{L}^j_{ac}\tilde{L}^{j*}_{bc} \times\left[1 - \cosh\left(\beta\frac{E_b - E_a - \mu(N_b - N_a)}{2}\right)\right] + \mathcal{O}\{\Gamma\delta\rho\}. \quad \text{(A2)}$$

Typically, the process j has a defined particle exchange. Thus, nonvanishing $\tilde{L}^j_{ac}$ and $\tilde{L}^{j*}_{bc}$ provide $N_b = N_a$. In the stationary state, we obtain

$$\delta\rho_{ba} = \frac{i}{E_a - E_b}\sum_{j,c}\Gamma_j\rho^0_{cc}\tilde{L}^j_{ac}\tilde{L}^{j*}_{bc} \times\left[1 - \cosh\left(\beta\frac{E_b - E_a}{2}\right)\right] + \mathcal{O}\{\Gamma^2\}. \quad \text{(A3)}$$

Thus, $\delta\rho_{ba}$ vanishes with decreasing coupling Γ. However, for $\beta|E_b - E_a| \gg 1$ the strong increase of the cosh appears to complicate the picture. As we show below, this is compensated by an exponential decay of $\rho_{cc}\tilde{L}^j_{ac}\tilde{L}^{j*}_{bc}$ in $\beta|E_b - E_a|$ provided the jump elements $\tilde{L}$ are bounded.

In order to show this, we assume $E_b > E_a$. We consider the state m with highest occupation, which has the effective energy $M = \mathrm{Min}_a(E_a - \mu N_a)$. Then, we find $\rho_{cc} \sim e^{\beta(\mu N_c - E_c - M)}$ and $E_b > E_a$ implies, $E_b - \mu N_b - M \geqslant E_b - E_a$. Now, we consider two cases

(1) if $E_b - \mu N_b < E_c - \mu N_c$ then $\rho_{cc} < e^{\beta(\mu N_b - E_b - M)} < e^{\beta(E_b - E_a)}$

(2) if $E_b - \mu N_b > E_c - \mu N_c$ then $f_j(E_b - E_c) \sim e^{-\beta[E_b - E_c - \mu(N_b - N_c)]}$

and we find

$$\begin{aligned}\rho_{cc}\tilde{L}^{j*}_{bc} &\lesssim e^{\beta(\mu N_c - E_c - M)}e^{-\beta[E_b - E_c - \mu(N_b - N_c)]/2}L^{j*}_{bc}\\ &< e^{\beta(\mu N_c - E_c - M)/2}e^{-\beta(E_b - \mu N_b - M)/2}L^{j*}_{bc}\\ &< e^{\beta(\mu N_c - E_c - M)/2}e^{-\beta(E_b - E_a)/2}L^{j*}_{bc}.\end{aligned}$$

In both cases, the exponential drop of $\rho_{cc}\tilde{L}^j_{ac}\tilde{L}^{j*}_{bc}$ in $\beta(E_b - E_a)$ compensates the increase in the cosh term. The case $E_a > E_b$ is analogous.

For the double-dot structure considered in Sec. III, we analytically find that in the equilibrium the coherences are bounded by coupling strength Γ. From Eq. (C7) for asymmetric junction $\Gamma_{L/R} = (1 \pm b)\Gamma$ we find

$$\rho_{11'} = \frac{b}{2}(\gamma^2 + i\gamma)\frac{(\bar{f}_+ + \bar{f}_-)s - (f_+ + f_-)\bar{s}}{1 + \gamma^2[1 - b^2(s + \bar{s})^2]}, \quad \text{(A4)}$$

which vanish for small Γ and in this case the equilibrium is reached. Here, the notation of Eq. (15) was used.

APPENDIX B: PARTICLE AND ENERGY CURRENTS

The average particle number $\langle\hat{N}\rangle$ in the system changes by

$$\begin{aligned}\tfrac{\partial}{\partial t}\langle\hat{N}\rangle &= \sum_b N_b\tfrac{\partial}{\partial t}\rho_{bb}\\ &= \sum_j\Gamma_j\Big(\sum_{baa'}N_b\tilde{L}^j_{ba}\rho_{aa'}\tilde{L}^{j*}_{ba'} - \sum_{bb'c}\frac{N_b}{2}\big[\rho_{bb'}\tilde{L}^{j*}_{cb'}\tilde{L}^j_{cb} + \tilde{L}^{j*}_{cb}\tilde{L}^j_{cb'}\rho_{b'b}\big]\Big), \quad \text{(B1)}\end{aligned}$$

where N_b denotes number of particles in the state b. Here, we used Eq. (4) together with the fact that the Hamiltonian $\hat{H}_{\rm eff}(t)$ does not change the particle number. Now, we rename the indices b,b',c by a,a',b in the second term and by a',a,b in the third term of the right-hand side of Eq. (B1), which results in

$$\frac{\partial}{\partial t}\langle\hat{N}\rangle = \sum_{j,baa'}\Gamma_j\Big(N_b - \frac{N_a + N_{a'}}{2}\Big)\tilde{L}^j_{ba}\rho_{aa'}\tilde{L}^{j*}_{ba'}. \quad \text{(B2)}$$

The jump operators $\hat{L}_j$ can be classified by the number Δ_j of electrons they transfer from the leads to the system. Correspondingly, negative Δ_j means the removal of particles. Assuming that there are no coherences $\rho_{aa'}$ between states with different particle number, we can replace $N_b - \frac{N_a + N_{a'}}{2} \to \Delta_j$. Then, all changes due to jump operators related to transitions with lead ℓ contribute to the current from this lead into the system:

$$I_\ell = \sum_{\substack{j\text{ related to }\ell\\ baa'}}\Gamma_j\Delta_j\tilde{L}^j_{ba}\rho_{aa'}\tilde{L}^{j*}_{ba'}. \quad \text{(B3)}$$

Similarly, we can calculate the energy current through the system. The energy of the system is defined as

$$E = \langle \hat{H}_S \rangle = \sum_{bb'} H_{bb'} \rho_{b'b} \tag{B4}$$

and its change is given by

$$\frac{\partial}{\partial t} E = i \sum_{bb'} H_{bb'} \langle b' | [\hat{\rho}, \hat{H}_{\text{eff}}(t)] | b \rangle + \sum_j \Gamma_j \left(\sum_{bb'aa'} H_{bb'} \tilde{L}^j_{b'a} \rho_{aa'} \tilde{L}^{j*}_{ba'} - \sum_{bb'b''c} \frac{H_{bb'}}{2} \left(\rho_{b'b''} \tilde{L}^{j*}_{cb''} \tilde{L}^j_{cb} + \tilde{L}^{j*}_{cb'} \tilde{L}^j_{cb''} \rho_{b''b} \right) \right). \tag{B5}$$

We split the first term with jump operators into two parts with exchanging $b \leftrightarrow b'$ in one of them and rename b,b',b'',c by a'',a,a',b in the second term and by a'',a',a,b in the third term, which results in

$$\frac{\partial}{\partial t} E = P_{\text{ext}}(t) + \sum_{j,baa'} \frac{\Gamma_j}{2} \left(K^j_{ba} \rho_{aa'} \tilde{L}^{j*}_{ba'} + \tilde{L}^{j*}_{ba} \rho_{aa'} K^j_{ba'} \right), \tag{B6}$$

where

$$K^j_{ba} = \sum_{b'} H_{bb'} \tilde{L}^j_{b'a} - \sum_{a'} \tilde{L}^j_{ba'} H_{a'a} \tag{B7}$$

and

$$P_{\text{ext}}(t) = i \langle [\hat{H}_S, \hat{H}_{\text{eff}}(t)] \rangle \tag{B8}$$

is the power transferred to the system from the outer fields. Now, if $\hat{H}_S$ is diagonal (i.e., $\hat{H}_S = \sum_b E_b |b\rangle\langle b|$) from Eq. (B6) we find the energy current from the lead ℓ:

$$\dot{E}_\ell = \sum_{\substack{j \text{ related to } \ell \\ baa'}} \Gamma_j \left(E_b - \frac{E_a + E_{a'}}{2} \right) \tilde{L}^j_{ba} \rho_{aa'} \tilde{L}^{j*}_{ba'}. \tag{B9}$$

APPENDIX C: ANALYTIC SOLUTIONS FOR THE DOUBLE-DOT SYSTEM

1. Transmission formalism

For the double-dot structure with no interactions $U = 0$ the transmission formalism [40–42] gives the following particle and energy currents flowing from the left lead (L) into the dots:

$$I_L = \frac{1}{2\pi} \int_{-\infty}^{\infty} dE \; \mathcal{T}(E) [f_L(E) - f_R(E)], \tag{C1}$$

$$\dot{E}_L = \frac{1}{2\pi} \int_{-\infty}^{\infty} dE \; \mathcal{T}(E) \, E \, [f_L(E) - f_R(E)], \tag{C2}$$

with $f_{L/R}(E) = [\exp(\frac{E-\mu_{L/R}}{T_{L/R}}) + 1]^{-1}$. For symmetric coupling $\Gamma_L = \Gamma_R = \Gamma$, the transmission function is

$$\mathcal{T}(E) = \left| \frac{\Gamma/2}{E - (V_g - \Omega) + i\Gamma/2} - \frac{\Gamma/2}{E - (V_g + \Omega) + i\Gamma/2} \right|^2. \tag{C3}$$

We note that the above expressions are valid for the leads having an infinite bandwidth.

2. PERLind approach

After inserting Γ_j and $\tilde{L}_j$ defined in Sec. III into Eq. (4), we obtain for noninteracting case $U = 0$ such equations:

$$\partial_t \boldsymbol{\rho} = \mathcal{L} \boldsymbol{\rho}, \quad \boldsymbol{\rho} = (\rho_{00} \quad \rho_{11} \quad \rho_{1'1'} \quad \rho_{22} \quad \rho_{11'} \quad \rho_{1'1})^T, \tag{C4}$$

with the Liouvillian $\mathcal{L}$

$$\mathcal{L} = \frac{\Gamma}{2} \begin{pmatrix} -F_+ - F_- & \bar{F}_- & \bar{F}_+ & 0 & \bar{S}_\delta & \bar{S}_\delta \\ F_- & -F_+ - \bar{F}_- & 0 & \bar{F}_+ & \frac{1}{2}(S_\delta - \bar{S}_\delta) & \frac{1}{2}(S_\delta - \bar{S}_\delta) \\ F_+ & 0 & -\bar{F}_+ - F_- & \bar{F}_- & \frac{1}{2}(S_\delta - \bar{S}_\delta) & \frac{1}{2}(S_\delta - \bar{S}_\delta) \\ 0 & F_+ & F_- & -\bar{F}_+ - \bar{F}_- & -S_\delta & -S_\delta \\ S_\delta & \frac{1}{2}(S_\delta - \bar{S}_\delta) & \frac{1}{2}(S_\delta - \bar{S}_\delta) & -\bar{S}_\delta & -2\left(1 - \frac{i}{\gamma}\right) & 0 \\ S_\delta & \frac{1}{2}(S_\delta - \bar{S}_\delta) & \frac{1}{2}(S_\delta - \bar{S}_\delta) & -\bar{S}_\delta & 0 & -2\left(1 + \frac{i}{\gamma}\right) \end{pmatrix}. \tag{C5}$$

Here, we have introduced the following notations:

$$\begin{aligned}
\Gamma &= \frac{1}{2}(\Gamma_L + \Gamma_R), \quad \gamma = \frac{\Gamma}{2\Omega}, \\
f_L(E) &= f_{\rm I}(E), \quad f_R(E) = f_{\rm III}(E), \quad \bar{f}_\ell(E) = 1 - f_\ell(E), \\
F_\pm &= \frac{1}{\Gamma}[\Gamma_L f_L(V_g \pm \Omega) + \Gamma_R f_R(V_g \pm \Omega)], \quad \bar{F}_\pm = \frac{1}{\Gamma}[\Gamma_L \bar{f}_L(V_g \pm \Omega) + \Gamma_R \bar{f}_R(V_g \pm \Omega)], \\
S_\ell &= \frac{\Gamma_\ell}{\Gamma}\sqrt{f_\ell(V_g + \Omega) f_\ell(V_g - \Omega)}, \quad \bar{S}_\ell = \frac{\Gamma_\ell}{\Gamma}\sqrt{\bar{f}_\ell(V_g + \Omega) \bar{f}_\ell(V_g - \Omega)}, \\
S_\delta &= S_L - S_R, \quad \bar{S}_\delta = \bar{S}_L - \bar{S}_R.
\end{aligned} \tag{C6}$$

We are interested in stationary-state solution of Eq. (C4). By setting $\partial_t \boldsymbol{\rho} = 0$ and imposing normalization condition $\mathrm{Tr}[\rho] = \rho_{00} + \rho_{11} + \rho_{1'1'} + \rho_{22} = 1$, we obtain the solution

$$\begin{aligned}
\rho_{00} &= \frac{1}{4}\bar{F}_+\bar{F}_- - \frac{1}{8}[(F_+ + F_-)S_\delta - (\bar{F}_+ + \bar{F}_-)\bar{S}_\delta - 4(S_\delta + \bar{S}_\delta)]\,\mathrm{Re}(\rho_{1'1}), \\
\rho_{11} &= \frac{1}{4}\bar{F}_+F_- + \frac{1}{8}[(F_+ + F_-)S_\delta - (\bar{F}_+ + \bar{F}_-)\bar{S}_\delta]\,\mathrm{Re}(\rho_{1'1}), \\
\rho_{1'1'} &= \frac{1}{4}F_+\bar{F}_- + \frac{1}{8}[(F_+ + F_-)S_\delta - (\bar{F}_+ + \bar{F}_-)\bar{S}_\delta]\,\mathrm{Re}(\rho_{1'1}), \\
\rho_{22} &= \frac{1}{4}F_+F_- - \frac{1}{8}[(F_+ + F_-)S_\delta - (\bar{F}_+ + \bar{F}_-)\bar{S}_\delta + 4(S_\delta + \bar{S}_\delta)]\,\mathrm{Re}(\rho_{1'1}), \\
\rho_{11'} &= \frac{1}{8}(\gamma^2 + i\gamma)\frac{(\bar{F}_+ + \bar{F}_-)S_\delta - (F_+ + F_-)\bar{S}_\delta}{1 + \gamma^2\left[1 - \left(\frac{S_\delta + \bar{S}_\delta}{2}\right)^2\right]}, \quad \rho_{1'1} = \rho^*_{11'}.
\end{aligned} \tag{C7}$$

Using the above expressions for the density matrix elements from Eqs. (B3) and (B9) we get such currents

$$I_L = \frac{1}{2}\frac{\Gamma_L\Gamma_R}{\Gamma_L + \Gamma_R}[g_+ + g_- - (s_L + s_R + \bar{s}_L + \bar{s}_R)2\,\mathrm{Re}(\rho_{1'1})], \tag{C8a}$$

$$\dot{E}_L = \frac{1}{2}\frac{\Gamma_L\Gamma_R}{\Gamma_L + \Gamma_R}[(V_g + \Omega)g_+ + (V_g - \Omega)g_- - V_g(s_L + s_R + \bar{s}_L + \bar{s}_R)2\,\mathrm{Re}(\rho_{1'1})], \tag{C8b}$$

where the following notation was introduced:

$$g_\pm = f_L(V_g \pm \Omega) - f_R(V_g \pm \Omega), \quad s_\ell = \sqrt{f_\ell(V_g + \Omega) f_\ell(V_g - \Omega)}, \quad \bar{s}_\ell = \sqrt{\bar{f}_\ell(V_g + \Omega) \bar{f}_\ell(V_g - \Omega)}. \tag{C9}$$

3. Redfield approach

After using Eq. (A3) of Ref. [48], we obtain the following Liouvillian for the first-order Redfield approach[2]:

$$\mathcal{L}_{\rm Red} = \frac{\Gamma}{2}\begin{pmatrix}
-F_+ - F_- & \bar{F}_- & \bar{F}_+ & 0 & \frac{\gamma'}{\gamma} - C^* & \frac{\gamma'}{\gamma} - C \\
F_- & -F_+ - \bar{F}_- & 0 & \bar{F}_+ & C^* & C \\
F_+ & 0 & -\bar{F}_+ - F_- & \bar{F}_- & C^* & C \\
0 & F_+ & F_- & -\bar{F}_+ - \bar{F}_- & -\frac{\gamma'}{\gamma} - C^* & -\frac{\gamma'}{\gamma} - C \\
\frac{\gamma'}{\gamma} + C & C & C & -\frac{\gamma'}{\gamma} + C & -2\left(1 - \frac{i}{\gamma}\right) & 0 \\
\frac{\gamma'}{\gamma} + C^* & C^* & C^* & -\frac{\gamma'}{\gamma} + C^* & 0 & -2\left(1 + \frac{i}{\gamma}\right)
\end{pmatrix}, \tag{C10}$$

where

$$\begin{aligned}
\gamma' &= \frac{\Gamma_L - \Gamma_R}{2 \times 2\Omega}, \\
C &= \frac{1}{2\pi i\Gamma}[(\Gamma_L\psi^*_{L+} - \Gamma_R\psi^*_{R+}) - (\Gamma_L\psi_{L-} - \Gamma_R\psi_{R-})], \\
\psi_{\ell\pm} &= \Psi\left(\frac{1}{2} + \frac{\mu_\ell - (V_g \pm \Omega)}{i2\pi T_\ell}\right).
\end{aligned} \tag{C11}$$

[2]In nonstationary state, the left-hand side of Eq. (A3) in Ref. [48] is replaced by $i\,\partial_t \rho_{bb'}$.

Here, $\Psi(z)$ denotes the digamma function [79]. We also used the notations introduced in Eqs. (C6) and (C9). For the stationary state $\mathcal{L}_{\rm Red}\boldsymbol{\rho} = 0$, we obtain the solution

$$\begin{aligned}
\rho_{00} &= \frac{1}{4}\bar{F}_+\bar{F}_- - \frac{1}{2}\,\mathrm{Re}\,(C\rho_{1'1}) - \frac{1}{4}\frac{\gamma'}{\gamma}(-2-\bar{F}_- - \bar{F}_+)\,\mathrm{Re}(\rho_{1'1}),\\
\rho_{11} &= \frac{1}{4}F_-\bar{F}_+ + \frac{1}{2}\,\mathrm{Re}\,(C\rho_{1'1}) + \frac{1}{4}\frac{\gamma'}{\gamma}(-2+F_- + F_+)\,\mathrm{Re}(\rho_{1'1}),\\
\rho_{1'1'} &= \frac{1}{4}F_+\bar{F}_- + \frac{1}{2}\,\mathrm{Re}\,(C\rho_{1'1}) + \frac{1}{4}\frac{\gamma'}{\gamma}(-2+F_- + F_+)\,\mathrm{Re}(\rho_{1'1}),\\
\rho_{22} &= \frac{1}{4}F_+F_- - \frac{1}{2}\,\mathrm{Re}\,(C\rho_{1'1}) - \frac{1}{4}\frac{\gamma'}{\gamma}(+2+F_- + F_+)\,\mathrm{Re}(\rho_{1'1}),\\
\rho_{11'} &= \rho^*_{1'1} = \frac{(i+\gamma)[4\gamma C - \gamma'(F_+F_- - \bar{F}_-\bar{F}_+)] - 4i\gamma'^2\,\mathrm{Im}\,C}{8(1+\gamma^2-\gamma'^2)}.
\end{aligned} \tag{C12}$$

The particle and energy currents are calculated using Eqs. (A9) and (A10) of Ref. [48][3]:

$$I_L = \frac{1}{2}\frac{\Gamma_L\Gamma_R}{\Gamma_L+\Gamma_R}[g_+ + g_- - 4\,\mathrm{Re}(\rho_{1'1})], \tag{C13}$$

$$\dot{E}_L = \frac{1}{2}\frac{\Gamma_L\Gamma_R}{\Gamma_L+\Gamma_R}[(V_g+\Omega)g_+ + (V_g-\Omega)g_- - 4V_g\,\mathrm{Re}(\rho_{1'1})]. \tag{C14}$$

The Pauli master-equation result is obtained by neglecting the coherence term $\mathrm{Re}(\rho_{1'1})$ in the above expressions. The result with no principal parts (Redfield, no $\mathcal{P}$) is obtained by neglecting the imaginary part of C in Eq. (C11).

APPENDIX D: KINETIC TENSORS FOR THE TWO-CHROMOPHORE SYSTEM

In this appendix we write the kinetic tensors used to generate the results of Fig. 4. The Redfield tensor is obtained using Eqs. (370)–(375) of Ref. [6]. We get slightly different numerical values than in Ref. [27] at $\lambda = 35$ cm and $T = 185$ K:

$$-K^{\rm Red} = \begin{pmatrix} -8.6 & 27.6 & 52.9 & 52.9 \\ 8.6 & -27.6 & -52.9 & -52.9 \\ 2.8+6.5i & -9.0-25.0i & -52.5+48.5i & 18.1+48.5i \\ 2.8-6.5i & -9.0+25.0i & 18.1-48.5i & -52.5-48.5i \end{pmatrix} \times 2\pi c/\mathrm{cm}. \tag{D1}$$

Here, $K^{\rm Red}$ corresponds to the reduced density matrix expressed as $\boldsymbol{\rho} = (\rho_{11}, \rho_{22}, \rho_{12}, \rho_{21})^T$. The secular approximation is obtained by removing all the terms from $K^{\rm Red}_{abcd}$ where $E_b - E_a \neq E_d - E_c$:

$$-K^{\rm Sec} = \begin{pmatrix} -8.6 & 27.6 & 0 & 0 \\ 8.6 & -27.6 & 0 & 0 \\ 0 & 0 & -52.5+48.5i & 0 \\ 0 & 0 & 0 & -52.5-48.5i \end{pmatrix} \times 2\pi c/\mathrm{cm}. \tag{D2}$$

We note that in simulations of Fig. 4 we have not used the imaginary parts of $K^{\rm Red}$ and $K^{\rm Sec}$, which correspond to neglecting the principal part $\mathcal{P}$ integrals. Our proposed Lindblad scheme as discussed in Sec. IV gives

$$-K^{\rm PERLind} = \begin{pmatrix} -8.6 & 27.6 & 17.0 & 17.0 \\ 8.6 & -27.6 & -17.0 & -17.0 \\ 7.4 & -26.6 & -52.5 & 15.4 \\ 7.4 & -26.6 & 15.4 & -52.5 \end{pmatrix} \times 2\pi c/\mathrm{cm}. \tag{D3}$$

Lastly, the procedure described in Ref. [27] from Eq. (D1) gives

$$-K^{\rm Palm} = \begin{pmatrix} -8.6 & 27.6 & 55.1 & 55.1 \\ 8.6 & -27.6 & -55.1 & -55.1 \\ -30.7 & 98.7 & -52.5 & -15.4 \\ -30.7 & 98.7 & -15.4 & -52.5 \end{pmatrix} \times 2\pi c/\mathrm{cm}. \tag{D4}$$

[3]In Eqs. (A9)–(A11), (B3), and (B4) of Ref. [48] the minus sign from the definition of the currents, Eq. (2), is missing. There, 2 Im has to be replaced by −2 Im.

APPENDIX E: SCATTERING MATRIX ELEMENTS FOR QCLs

1. Electron-phonon interaction

For the polar interaction with longitudinal optical phonons, the function $g_{\mathbf{q},q_z}$ in the Fröhlich Hamiltonian (26) reads as [71]

$$g_{\mathbf{q},q_z} = \frac{i}{\sqrt{AL}}\sqrt{\frac{e^2\hbar\omega_{\mathrm{LO}}}{2\epsilon_0\epsilon_p}}\frac{1}{\sqrt{\mathbf{q}^2+q_z^2}}, \tag{E1}$$

where L is the normalization length determining the q_z spacing, ω_{LO} is the longitudinal optical phonon frequency, which is assumed to be constant, and ϵ_0 is the vacuum permittivity. Also, $\epsilon_p^{-1} = \epsilon_\infty^{-1} - \epsilon_s^{-1}$, where ϵ_∞ and ϵ_s are the relative dielectric constants evaluated far above and far below ω_{LO}, respectively.

Now, we evaluate Eq. (29) for the emission process. From the first term of Eq. (28) we find

$$\Gamma^{\mathrm{em.}}_{\alpha\mathbf{k}\to\beta\mathbf{k}+\mathbf{q}} = \frac{2\pi}{\hbar}\frac{1}{A}\frac{e^2\hbar\omega_{\mathrm{LO}}}{2\epsilon_0\epsilon_p}[f_B(\hbar\omega_{\mathrm{LO}})+1] \times\int\frac{dq_z}{2\pi}\frac{\left|M^{q_z}_{\beta\alpha}\right|^2}{\mathbf{q}^2+q_z^2}\delta\left(\Delta_{\beta\alpha,\mathbf{q}}+\frac{\hbar^2}{m_c}\mathbf{k}\cdot\mathbf{q}+\hbar\omega_{\mathrm{LO}}\right), \tag{E2}$$

where we used the continuum limit $\sum_{q_z}\to\frac{L}{2\pi}\int dq_z$ and introduced $\Delta_{\beta\alpha,\mathbf{q}} = E_\beta - E_\alpha + E_{\mathbf{q}}$. We assume that the in-plane electron states have thermal occupations, i.e., $f_{\alpha,\mathbf{k}}\propto e^{-E_{\mathbf{k}}/(k_{\mathrm{B}}T)}$. In such a case, Eqs. (29) and (E2) give the following emission rate:

$$R^{\mathrm{em.}}_{\alpha\to\beta} = C_-\int\frac{dq_z}{2\pi}\int_0^\infty\frac{dq}{2\pi}\frac{\exp\left[-\frac{(\Delta_{\beta\alpha,\mathbf{q}}+\hbar\omega_{\mathrm{LO}})^2}{4E_{\mathbf{q}}k_{\mathrm{B}}T}\right]}{\mathbf{q}^2+q_z^2}\left|M^{q_z}_{\beta\alpha}\right|^2, \tag{E3}$$

where $C_\pm = \pm f_B(\pm\hbar\omega_{\mathrm{LO}})\frac{2\pi}{\hbar}\frac{e^2\hbar\omega_{\mathrm{LO}}}{2\epsilon_0\epsilon_p}\sqrt{\frac{m_c}{2\pi\hbar^2k_{\mathrm{B}}T}}$. Here, we performed the $\mathbf{k}$ sums using the continuum limit $\sum_{\mathbf{k}}\to\frac{A}{(2\pi)^2}\int d^2k = \frac{A}{(2\pi)^2}\int_0^{2\pi}d\phi\int_0^{+\infty}dk\,k$ and by identifying $\mathbf{k}\cdot\mathbf{q} = kq\cos(\phi)$. Also, the following integral was used:

$$\int_0^{2\pi}d\phi\,\sec^2(\phi)e^{-a\sec^2(\phi)}\overset{a>0}{=}2e^{-a}\sqrt{\frac{\pi}{a}}. \tag{E4}$$

The emission rate (E3) has the form of Eq. (30) with

$$f^{\mathrm{em.}}_{q_z}(E_\beta-E_\alpha) = \frac{C_-}{L}\int_0^\infty\frac{dq}{2\pi}\frac{\exp\left[-\frac{(\Delta_{\beta\alpha,\mathbf{q}}+\hbar\omega_{\mathrm{LO}})^2}{4E_{\mathbf{q}}k_{\mathrm{B}}T}\right]}{\mathbf{q}^2+q_z^2}, \tag{E5}$$

which agrees with the result found by Gordon and Majer [33] up to a factor of 2.

For phonon absorption, we need to change the sign of $\hbar\omega_{\mathrm{LO}}$ in the delta function and change $f_B(\hbar\omega_{\mathrm{LO}})+1\to f_B(\hbar\omega_{\mathrm{LO}})$, resulting in

$$f^{\mathrm{abs.}}_{q_z}(E_\beta-E_\alpha) = \frac{C_+}{L}\int_0^\infty\frac{dq}{2\pi}\frac{\exp\left[-\frac{(\Delta_{\beta\alpha,\mathbf{q}}-\hbar\omega_{\mathrm{LO}})^2}{4E_{\mathbf{q}}k_{\mathrm{B}}T}\right]}{\mathbf{q}^2+q_z^2}. \tag{E6}$$

In the simulations of Figs. 5 and 6, we used the standard GaAs semiconductor material parameters: $m_c = 0.067m_e$, $\hbar\omega_{\mathrm{LO}} = 36.7$ meV, $\epsilon_s = 13.0$, $\epsilon_\infty = 10.89$, $\epsilon_p = 67.09$. Here, m_e denotes the mass of electron.

2. Scattering by impurities

For impurity scattering, we have the following momentum-resolved transition rate:

$$\Gamma_{\alpha\mathbf{k}\to\beta\mathbf{k}+\mathbf{q}} = \frac{2\pi}{\hbar}|\langle U_{\beta\alpha,\mathbf{q}}\rangle|^2\delta(E_{\beta,\mathbf{k}+\mathbf{q}}-E_{\alpha,\mathbf{k}}), \tag{E7}$$

where

$$|\langle U_{\beta\alpha,\mathbf{q}}\rangle|^2 = AN_{2\mathrm{D}}\sum_i w_i V^i_{\beta\alpha,\mathbf{q}}V^i_{\alpha\beta,-\mathbf{q}} \tag{E8}$$

is an impurity average for electron scattering and $N_{2\mathrm{D}}$ is the total impurity density per period with w_i being a normalized weight function distributing it on different positions z_i within each period. Here,

$$V^i_{\beta\alpha,\mathbf{q}} = -\frac{e^2}{2\epsilon_0\epsilon_s A}\frac{\exp(-i\,\mathbf{q}\cdot\mathbf{r}_i)}{\sqrt{q^2+\lambda^2}}M^{i,q}_{\beta\alpha}, \tag{E9}$$

where λ is the inverse screening length and

$$M^{i,q}_{\beta\alpha} = \int dz\,\psi^*_\beta(z)\psi_\alpha(z)e^{-\sqrt{q^2+\lambda^2}|z-z_i|}. \tag{E10}$$

Using Eq. (29), we perform the thermal average over the in-plane momentum ($f_{\alpha,\mathbf{k}}\propto e^{-E_{\mathbf{k}}/(k_{\mathrm{B}}T)}$) and obtain

$$R_{\alpha\to\beta} = \sum_i D\int_0^\infty\frac{dq}{2\pi}\left|M^{i,q}_{\beta\alpha}\right|^2 f_{i,q}(E_\beta-E_\alpha) = \sum_{i,q}\left|M^{i,q}_{\beta\alpha}\right|^2 f_{i,q}(E_\beta-E_\alpha), \tag{E11}$$

where

$$f_{i,q}(E_\beta-E_\alpha) = \frac{2\pi}{D\hbar}w_iN_{2\mathrm{D}}\left(\frac{e^2}{2\epsilon_0\epsilon_s}\right)^2\sqrt{\frac{m_c}{2\pi\hbar^2k_{\mathrm{B}}T}} \times\frac{\exp\left[-\frac{\Delta^2_{\beta\alpha,q}}{4E_qk_{\mathrm{B}}T}\right]}{q^2+\lambda^2}, \tag{E12}$$

where D is an arbitrary length scale to get the dimensions right. As for phonon scattering, the scattering rate in Eq. (E11) can thus be generalized to the Lindblad tensors of Eq. (5) with $L^{i,q}_{ab} = M^{i,q}_{ab}$ and distribution function $f_{i,q}(E_a-E_b)$. For the simulations we used $N_{2\mathrm{D}} = 5.16\times10^{10}$ cm^{-2}, five impurity layers per period with $w_i = 0.2$ at positions $z_i\in\{42.0,44.8,47.7,50.6,53.4\}$ nm, and Lindhard static screening length of $\lambda^{-1}\in\{24.3,30.0,33.5,38.5\}$ nm at $T\in\{77,120,150,200\}$ K.

[1] F. Bloch, Phys. Rev. **70**, 460 (1946).
[2] M. A. Kastner, Rev. Mod. Phys. **64**, 849 (1992).
[3] L. P. Kouwenhoven, C. M. Marcus, P. L. Mceuen, S. Tarucha, R. M. Westervelt, and N. S. Wingreen, in *Mesoscopic Electron Transport*, edited by L. L. Sohn, L. P. Kouwenhoven, and G. Schön, NATO Advanced Study Institutes, Ser. E: Applied Sciences, Vol. 345 (Kluwer, Dordrecht, 1997).
[4] S. M. Reimann and M. Manninen, Rev. Mod. Phys. **74**, 1283 (2002).
[5] R. Hanson, J. R. Petta, S. Tarucha, and L. M. K. Vandersypen, Rev. Mod. Phys. **79**, 1217 (2007).
[6] D. Abramavicius, B. Palmieri, D. V. Voronine, F. Šanda, and S. Mukamel, Chem. Rev. **109**, 2350 (2009).
[7] A. Ishizaki and G. R. Fleming, Annu. Rev. Condens. Matter Phys. **3**, 333 (2012).
[8] L. Esaki and R. Tsu, IBM J. Res. Dev. **14**, 61 (1970).
[9] A. Wacker, Phys. Rep. **357**, 1 (2002).
[10] R. C. Iotti, E. Ciancio, and F. Rossi, Phys. Rev. B **72**, 125347 (2005).
[11] J. Faist, F. Capasso, D. L. Sivco, C. Sirtori, A. L. Hutchinson, and A. Y. Cho, Science **264**, 553 (1994).
[12] C. Jirauschek and T. Kubis, Appl. Phys. Rev. **1**, 011307 (2014).
[13] C. Timm, Phys. Rev. B **77**, 195416 (2008).
[14] J. E. Subotnik, T. Hansen, M. A. Ratner, and A. Nitzan, J. Chem. Phys. **130**, 144105 (2009).
[15] G. Schaller, P. Zedler, and T. Brandes, Phys. Rev. A **79**, 032110 (2009).
[16] D. Taj, R. C. Iotti, and F. Rossi, Eur. Phys. J. B **72**, 305 (2009).
[17] S. Koller, M. Grifoni, M. Leijnse, and M. R. Wegewijs, Phys. Rev. B **82**, 235307 (2010).
[18] M. Esposito and M. Galperin, J. Phys. Chem. C **114**, 20362 (2010).
[19] L. Chen, T. Hansen, and I. Franco, J. Phys. Chem. C **118**, 20009 (2014).
[20] R. K. Wangsness and F. Bloch, Phys. Rev. **89**, 728 (1953).
[21] A. G. Redfield, IBM J. Res. Dev. **1**, 19 (1957).
[22] C. Weber, A. Wacker, and A. Knorr, Phys. Rev. B **79**, 165322 (2009).
[23] A. Pan, B. A. Burnett, C. O. Chui, and B. S. Williams, Phys. Rev. B **96**, 085308 (2017).
[24] G. Lindblad, Commun. Math. Phys. **48**, 119 (1976).
[25] V. Gorini, A. Kossakowski, and E. C. G. Sudarshan, J. Math. Phys. **17**, 821 (1976).
[26] H.-P. Breuer and F. Petruccione, *Open Quantum Systems* (Oxford University Press, Oxford, 2006).
[27] B. Palmieri, D. Abramavicius, and S. Mukamel, J. Chem. Phys. **130**, 204512 (2009).
[28] A. Wacker and A.-P. Jauho, Phys. Rev. Lett. **80**, 369 (1998).
[29] H. Callebaut and Q. Hu, J. Appl. Phys. **98**, 104505 (2005).
[30] R. Rosati, D. E. Reiter, and T. Kuhn, Phys. Rev. B **95**, 165302 (2017).
[31] R. Rosati, R. C. Iotti, F. Dolcini, and F. Rossi, Phys. Rev. B **90**, 125140 (2014).
[32] O. Hod, C. A. Rodríguez-Rosario, T. Zelovich, and T. Frauenheim, J. Phys. Chem. A **120**, 3278 (2016).
[33] A. Gordon and D. Majer, Phys. Rev. B **80**, 195317 (2009).
[34] Y. V. Pershin, Y. Dubi, and M. Di Ventra, Phys. Rev. B **78**, 054302 (2008).
[35] S. A. Gurvitz and Y. S. Prager, Phys. Rev. B **53**, 15932 (1996).
[36] S. A. Gurvitz, Phys. Rev. B **57**, 6602 (1998).
[37] T. Novotný, Europhys. Lett. **59**, 648 (2002).
[38] A. Levy and R. Kosloff, Europhys. Lett. **107**, 20004 (2014).
[39] B. Sothmann, R. Sánchez, and A. N. Jordan, Nanotechnology **26**, 032001 (2015).
[40] C. Caroli, R. Combescot, P. Nozieres, and D. Saint-James, J. Phys. C: Solid State Phys. **4**, 916 (1971).
[41] M. Büttiker, Y. Imry, R. Landauer, and S. Pinhas, Phys. Rev. B **31**, 6207 (1985).
[42] S. Datta, *Electronic Transport in Mesoscopic Systems* (Cambridge University Press, Cambridge, 1995).
[43] U. Harbola, M. Esposito, and S. Mukamel, Phys. Rev. B **74**, 235309 (2006).
[44] M. G. Schultz and F. von Oppen, Phys. Rev. B **80**, 033302 (2009).
[45] P. P. Hofer, M. Perarnau-Llobet, L. D. M. Miranda, G. Haack, R. Silva, J. B. Brask, and N. Brunner, New J. Phys. **19**, 123037 (2017).
[46] G. Kiršanskas, J. N. Pedersen, O. Karlström, M. Leijnse, and A. Wacker, Comput. Phys. Commun. **221**, 317 (2017).
[47] R. Hussein and S. Kohler, Phys. Rev. B **89**, 205424 (2014).
[48] K. M. Seja, G. Kiršanskas, C. Timm, and A. Wacker, Phys. Rev. B **94**, 165435 (2016).
[49] R. Alicki, Rep. Math. Phys. **10**, 249 (1976).
[50] G. S. Agarwal, Z. Phys. **258**, 409 (1973).
[51] H. J. Carmichael and D. F. Walls, Z. Phys. B **23**, 299 (1976).
[52] A. Kossakowski, A. Frigerio, V. Gorini, and M. Verri, Commun. Math. Phys. **57**, 97 (1977).
[53] W. A. Majewski, J. Math. Phys. **25**, 614 (1984).
[54] F. Fagnola and V. Umanità, Math. Notes **84**, 108 (2008).
[55] J. Faist, *Quantum Cascade Lasers* (Oxford University Press, Oxford, 2013).
[56] M. S. Vitiello, G. Scalari, B. Williams, and P. D. Natale, Opt. Express **23**, 5167 (2015).
[57] S.-C. Lee, F. Banit, M. Woerner, and A. Wacker, Phys. Rev. B **73**, 245320 (2006).
[58] D. Calecki, J. F. Palmier, and A. Chomette, J. Phys. C: Solid State Phys. **17**, 5017 (1984).
[59] S. Tortora, F. Compagnone, A. Di Carlo, P. Lugli, M. T. Pellegrini, M. Troccoli, and G. Scamarcio, Phys. B (Amsterdam) **272**, 219 (1999).
[60] C. Jirauschek, G. Scarpa, P. Lugli, M. S. Vitiello, and G. Scamarcio, J. Appl. Phys. **101**, 086109 (2007).
[61] K. Donovan, P. Harrison, and R. W. Kelsall, Appl. Phys. Lett. **75**, 1999 (1999).
[62] S. Kumar and Q. Hu, Phys. Rev. B **80**, 245316 (2009).
[63] E. Dupont, S. Fathololoumi, and H. C. Liu, Phys. Rev. B **81**, 205311 (2010).
[64] R. Terazzi and J. Faist, New J. Phys. **12**, 033045 (2010).
[65] R. C. Iotti and F. Rossi, Phys. Rev. Lett. **87**, 146603 (2001).
[66] I. Waldmueller, W. W. Chow, E. W. Young, and M. C. Wanke, IEEE J. Quantum Electron. **42**, 292 (2006).
[67] T. Schmielau and M. F. Pereira, Appl. Phys. Lett. **95**, 231111 (2009).
[68] T. Kubis, C. Yeh, P. Vogl, A. Benz, G. Fasching, and C. Deutsch, Phys. Rev. B **79**, 195323 (2009).
[69] G. Hałdaś, A. Kolek, and I. Tralle, IEEE J. Quantum Electron. **47**, 878 (2011).
[70] A. Wacker, M. Lindskog, and D. O. Winge, IEEE J. Sel. Top. Quantum **19**, 1200611 (2013).

[71] O. Madelung, *Introduction to Solid-State Theory* (Springer, Berlin, 1978).
[72] L. Li, L. Chen, J. Zhu, J. Freeman, P. Dean, A. Valavanis, A. G. Davies, and E. H. Linfield, Electron. Lett. **50**, 309 (2014).
[73] M. Lindskog, D. O. Winge, and A. Wacker, Proc. SPIE **8846**, 884603 (2013).
[74] S. Kohen, B. Williams, and Q. Hu, J. Appl. Phys. **97**, 053106 (2005).
[75] J. T. Lü and J. C. Cao, Appl. Phys. Lett. **88**, 061119 (2006).
[76] R. C. Iotti, F. Rossi, M. S. Vitiello, G. Scamarcio, L. Mahler, and A. Tredicucci, Appl. Phys. Lett. **97**, 033110 (2010).
[77] Y. B. Shi and I. Knezevic, J. Appl. Phys. **116**, 123105 (2014).
[78] J. D. Hunter, Comput. Sci. Eng. **9**, 90 (2007), available at http://matplotlib.org
[79] M. Abramowitz and I. A. Stegun, *Handbook of Mathematical Functions* (National Bureau of Standards, Washington, DC, 1972).